



UNIVERSITAT
POLITÈCNICA
DE VALÈNCIA



UNIVERSITAT POLITÈCNICA DE VALÈNCIA

School of Design Engineering

Design of a structural health monitoring system based on
energy harvesting.

End of Degree Project

Bachelor's Degree in Industrial Electronics and Automation
Engineering

AUTHOR: Morellá Campos, Álvaro

Tutor: Patrao Herrero, Iván

Cotutor: Limeres García, Cristina

ACADEMIC YEAR: 2022/2023



UNIVERSITAT
POLITÈCNICA
DE VALÈNCIA

UNDERGRADUATE THESIS
INDUSTRIAL ELECTRONICS AND AUTOMATION ENGINEERING

DESIGN OF A STRUCTURAL HEALTH MONITORING SYSTEM BASED ON ENERGY HARVESTING

ÁLVARO MORELLÁ CAMPOS



Escuela Técnica Superior de Ingeniería del Diseño

UNIVERSITAT POLITÈCNICA DE VALÈNCIA

UNDERGRADUATE THESIS PROJECT

Design of a Structural Health Monitoring system based on Energy Harvesting

Author
ÁLVARO MORELLÁ CAMPOS

Tutors
IVÁN PATRAO
CRISTINA LIMERES

July 2023



UNIVERSITAT
POLITÈCNICA
DE VALÈNCIA



Escuela Técnica Superior de Ingeniería del Diseño

Acknowledgments

I don't think there are enough words to show how grateful I am to all the people who have helped me throughout my life to overcome all the obstacles I have encountered and who have allowed me to achieve my goals.

First of all, I would like to thank my parents: my father for instilling in me scientific curiosity with all the experiments we did together when I was little; and my mother for always helping me to get up when I was at my lowest. I would not be here if it were not for both of you.

I would also like to thank my dearest friends from college. To Pablo Fernández, Joaquim Cànoves, Isabel Fernández and Rafaele Perminaité. Thank you for the days at the UPV, for all those hours of working together in the windows of Pablo's terrace, for the unconditional help I have received from you and for the moments we have spent these last four years (and those to come, you will not get rid of me that easily).

Also to my friends from Sorbonne and the Erasmus in Paris for one of the best years of my life. Thank you for making me laugh even on the hardest days and for making me want to stay at the university until late at night. Thank you also for accompanying me in the libraries of Jussieu while I was doing this thesis, for the trips, the "family dinners" and the evenings of cards in the gardens of "Invalides" (which will have to be repeated when I come to visit you). If getting to know Paris and living there has been so wonderful, I am sure it has been thanks to you. You have become part of my family in a very short time and I am sure you will remain so forever.

Last but not least, I want to thank my second family, my friends from Jérica (Castellón, Spain). I could not thank you enough for all the moments we have spent together even if I was allowed to write a book of acknowledgments. Since we have been together (which is since we were born), you have been a very important part of my life, and I am completely sure that this will continue, even if we each end up in a different city (or country).

To all of you that I have mentioned and to those that I have not due to lack of space on this page (and not because I have less to thank you for), thank you. This thesis is dedicated to you and, although it has my name on it, it is as much yours as it is mine.

Álvaro Morellá Campos
UPV, July 2023

ABSTRACT

This document collects the undergraduate thesis project of the Degree in Industrial Electronics and Automation Engineering, which is based on the design of a Structural Health Measurement system for a bridge.

With the improvement of new technologies, engineers around the world have been trying to create the most efficient ways to improve the performance of all their creations. In this case, the control of structure's health is a very interesting way of maintaining the good shape of all the civil structures that are used every day and checking their integrity as well as redefining the limits to which they can be held. Specially with everyday use structures, we have had the opportunity to realise that many of the high cost works that have been carried on could have been easily prevented by periodically checking their main parts and their reaction to normal wear and tear.

The aim of this project is to design a Structural Health Monitoring system for the permanent control of the tension in the cables of the Assut de l'Or cable-stayed bridge situated on the Turia river gardens in the city of València (Spain). This system is based on the "energy harvesting" as far as power supply is concerned, and with the purpose of eliminating all costly wired connections , all the data from the different parts of the system will be available for wireless retrieval.

RESUMEN

Este documento recopila el procedimiento para la realización del Trabajo de Final del Grado en Ingeniería Electrónica Industrial y Automática, que se basa en el diseño de un sistema de Medición de la Salud Estructural de un puente.

Con la mejora de las nuevas tecnologías, los ingenieros de todo el mundo investigan formas más eficientes de mejorar el comportamiento y la resistencia de todas sus construcciones. En este caso, el control de la salud de estructuras es una forma muy interesante de mantener en buena forma todas las construcciones usadas cada día y tanto comprobar su integridad como redefinir los límites hasta los que pueden ser llevadas. Especialmente en estructuras de uso diario, hemos tenido la oportunidad de comprobar que la mayoría de las costosas reparaciones que han tenido que ser llevadas a cabo podrían haber sido fácilmente evitadas con un análisis periódico de sus partes principales y de su reacción al desgaste normal.

El objetivo de este proyecto es el de diseñar un sistema de Medición de la Salud Estructural para controlar permanentemente la tensión de los cables del puente atirantado "Assut de l'Or", situado en el antiguo cauce del río Turia, en la ciudad de València (España). Este sistema está basado en el concepto del "energy harvesting" en lo que a alimentación eléctrica concierne, y con el propósito de eliminar toda costosa comunicación cableada en mente, todos los datos recogidos por el conjunto de sensores del puente podrán ser recuperados de forma inalámbrica.

RESUM

Aquest document recopila el procediment per a la realització del Treball de Final del Grau en Enginyeria Electrònica Industrial i Automàtica, que es basa en el disseny d'un sistema de Mesurament de la Salut Estructural d'un pont.

Amb la millora de les noves tecnologies, els enginyers de tot el món investiguen formes més eficients de millorar el comportament i la resistència de totes les seues construccions. En aquest cas, el control de la salut d'estructures és una forma molt interessant de mantindre en bona forma totes les construccions usades cada dia i tant comprovar la seua integritat com redefinir els límits fins als quals poden ser portades. Especialment en estructures d'ús diari, hem tingut l'oportunitat de comprovar que la majoria de les costoses reparacions que han hagut de ser dutes a terme podrien haver sigut fàcilment evitades amb una anàlisi periòdic de les seues parts principals i del seu regambal al desgast normal.

L'objectiu d'aquest projecte és el de dissenyar un sistema de Mesurament de la Salut Estructural per a controlar permanentment la tensió dels cables del pont atirantat "Assut de l'Or", situat en l'antic llit del riu Túria, a la ciutat de València (Espanya). Aquest sistema està basat en el concepte del "energy harvesting" en el que a alimentació elèctrica concerneix, i amb el propòsit d'eliminar tota costosa comunicació cablejada en ment, totes les dades recollides pel conjunt de sensors del pont estaran disponibles per a ser recuperats de manera sense fil.

Documents

I	Technical Report	5
II	Plans	67
III	Written specifications	83
IV	Budget	93

List of Figures

1	Diagram of an SHM system on a bridge	12
2	Example of sensors used in bridge SHM	12
3	Diagram of Energy Harvesting systems	15
4	Two of the predecessors of Energy Harvesting	16
5	Diagram of a solar cell based EH system	17
6	I-V and P curve of a solar panel	18
7	I-V and P curve of a solar panel	20
8	View of the bridge in the Arts and Sciences City	21
9	Dimension diagram of the <i>Assut de l'Or</i> bridge	22
10	Diagram of the different construction and sheathing type of the cables	23
11	Details of the sensor location	24
12	Sketch of the placement of the sensor in the anchorage	28
13	A Vibrating Wire Strain Gauge installed on a steel rod	29
14	Diagram of a film strain gauge	30
15	Diagram of the HBM Full-Bridge Strain Gauges	31
16	Diagram of the OMEGA SGT-3G/350-FB41 Strain Gauge	31
17	Wheatstone bridge representations	32
18	Dummy gauge in perpendicular configuration for temperature compensation	33
19	STMicroelectronics SPV1050 Integrated Circuit (from datasheet)	34
20	Specifications table from SPV1050's datasheet	35
21	Instrumentation bridge used in the project	39
22	Schematic diagrams of the references in <i>Eagle</i>	44
23	Schematic diagram of the Instrumentation Amplifier in <i>Eagle</i>	44

24	Schematic diagram of the LPF designed in the Texas Instruments suite	45
25	Bode Diagrams of the system	46
26	Schematic diagram of the LPF in <i>Eagle</i>	46
27	Schematic diagram of the subtractor circuit	47
28	Schematic diagram of the offset subtractor in <i>Eagle</i>	48
29	Schematic diagram of the USB isolator in <i>Eagle</i>	49
30	Schematic diagram of the UART interface in <i>Eagle</i>	50
31	Regular buck-boost application of the SPV1050	51
32	Close-up view of the components in the battery management section	52
33	Close-up view of the components in the MPPT setting section	54
34	Schematic diagram of the SPV1050 assembly in <i>Eagle</i>	57
35	Render of the Power circuit in <i>Fusion360</i>	58
36	Fusion 360 Renders of the PCB	59
37	Side view render of the PCB in <i>Fusion360</i>	59
38	Temperature profile for reflux soldering of PCBs [1]	89

List of Tables

4.1	Comparison between three Power IC models	34
5.1	Dimensions of the cables for further calculations	38
1.1	Breakdown of the hours spent in this project and its economical correspondence	96
1.3	Total cost of the fabrication and assembly of the PCB	98
1.4	Amortization of the equipment and software	99
2.1	Total gross cost of the project	101
2.2	Net total cost of the project	101
3.2	Gross total per unit of a 30 unit production	104
3.3	Total cost per unit of a 30 unit production	104

Part I
Technical Report

Index of the Technical Report

1	Introduction	9
1.1	Objectives	9
2	Preliminary concepts	11
2.1	Structural Health Monitoring	11
2.1.1	History and examples	11
2.1.2	Benefits	13
2.1.3	Application in this project	13
2.2	Energy harvesting	15
2.2.1	History and examples	15
2.2.2	Benefits	16
2.2.3	Application in this project	17
3	Needs Assessment	21
3.1	Summary of the structure's specifications	22
3.1.1	Dimensions	22
3.1.2	Distribution of cables	22
3.1.3	Architecture of the cables	23
3.1.4	Placement of the system	24
3.2	Study of needs and factors to be considered (limitations and conditioning factors)	25
3.2.1	Precision	25
3.2.2	Noise rejection ratio	25
3.2.3	Independence from the grid	25
3.2.4	Continuous operation	26
3.2.5	Resistance to weather harshness	26
4	Alternative solutions and justification of the adopted solution	27
4.1	Measurement magnitude	27

4.2	Sensor location	28
4.3	Type of sensor	28
4.3.1	Strain Gauge and its application	30
4.4	Power managing	33
5	Detailed description of the solution adopted	37
5.1	Measurement magnitude	37
5.2	Signal conditioning	39
5.2.1	Instrumentation Bridge: adaptation of signal voltage range	39
5.2.2	Instrumentation amplifier	42
5.2.3	Low-pass filter	45
5.2.4	Subtraction of the 1.5V reference	47
5.3	Processing of the signal	49
5.3.1	Programming the μ Controller	49
5.3.2	Analog to Digital Converter	50
5.4	Power Source	50
5.4.1	DC-DC Converter	51
5.5	PCB	59
6	Conclusions	61
6.1	Note from the author	61
6.2	Future work	61
6.3	Sustainable Development Goals	62

1 | Introduction

1.1 Objectives

The objective of this undergraduate thesis is to design a reliable, grid-independent and easy to implement system that will permanently measure the tension in the stay-cables of the *Assut de l'Or* bridge for the evaluation of its current state and its response to normal use.

This system is aimed to ensure the safety of the structure and its surroundings as well as the users while maintaining the least invasive approach for this purpose. Also, taking into account its usefulness in the academic field for the creation of structural models with real data, the system will be designed to collect data in case of interest.

In order to measure the fulfillment of these objectives, we established the following key points:

- To evaluate the most interesting magnitude and location to measure in a cable-stayed bridge. Before the design of the system, the magnitude and location that will be used for the measurement of the structural health of the bridge will be determined. This is a very important key point, as the implementation of the system could be simpler or more complicated depending on these parameters.
- To design a signal conditioning system that allows for the correct reading of the magnitude. As the changes in the measurements of the sensor will likely be significantly small, a good conditioning stage will be needed. From amplifiers to filters, different elements will be applied to ensure the correct operation of the system.
- To design a power supply that will make the system independent from the electrical grid. Due to the fact that the bridge is already constructed, an independent power supply system will be needed. This will ensure a continuous operation as well as minimizing the aesthetic and structural impact on the bridge. An energy-harvesting based system will be implemented with a solar panel and a battery.
- To design a wireless communication system for complete independence from wired connections. The implementation of a wireless communications μ Controller will ensure the comfortable and reliability of the system while also ensuring the complete independence from wired communications to minimize, as in the case of the power supply, the impact on the structure in which the system is to be installed.
- To implement all the stages of the SHM system in a printed circuit board (PCB). This will allow for an easier and more space-efficient installation in the bridge. Moreover, the design of this PCB will ensure that the system is small enough for utilizing in different conditions should it need to be modified for its implementation in other structures.

2 | Preliminary concepts

2.1 Structural Health Monitoring

Structural Health Monitoring (SHM) is usually defined as the implementation of damage identification methods in aerospace, mechanical and civil structures [2].

These methods, specially known in civil structure surveillance, consists on the implementation of devices that deliver information about the state of the structure. The devices used for this purpose vary from rudimentary instruments like steel rulers or plastic crack measuring devices to more complex electronic systems like strain gauges, accelerometers or vibration sensors.

These methods, although commonly used for safety ensuring measures and quality control tests, can also provide a great data set for model developing, which can later be used by companies and universities so as to improve the designs and construction methods of said structures and their response to natural disasters like earthquakes [3].

2.1.1 History and examples

Interpreting literally the definition of SHM, the observation of the evolution of structures (especially civil ones, such as buildings, bridges, tunnels, etc.) has been present for centuries.

There have always been rudimentary checks of machinery, such as tapping on the chassis or wheels of a train to detect failures.

It has not been until the last decades when, thanks to the evolution of new technologies, the miniaturization of electronic sensing and processing devices and the new techniques of mathematical and statistical calculation when we have put into practice all the tools in the control of the health of our structures and this has gone from being qualitative to completely quantitative [2].

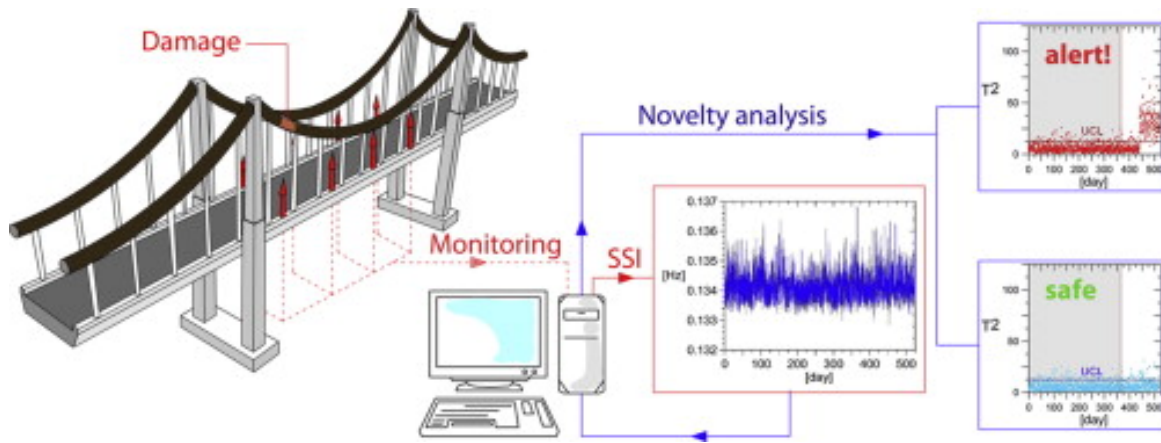


Figure 1: Diagram of an SHM system on a bridge [4]

In fact, although it may vary through different kinds of structures, in the case at hand (cable-stayed bridges), the first sensor-based systems were implemented around the decade of the 1990s, although their main appearance wasn't until the 2000s [5].

Since the change of decade, many SHM systems have been implemented around the world, specially in cable-stayed bridges in Asia (China, Japan and Korea), Europe and North America.

Many examples come to light when we talk about SHM, especially related to the present case:

- Shandong Binzhou Yellow River Bridge, China
- Rügen Bridge, Germany
- Adige Bridge, Italy
- ANZAC Bridge, Australia



Figure 2: Example of sensors used in bridge SHM [6]

2.1.2 Benefits

Many benefits can be related to the usage of these SHM systems, but the most important ones are, of course, safety and economics.

The periodical control of daily-use structures ensure the safety of the users and the integrity of said structures, and allows for anticipation for possible damages or failures. This is specially important on cable-stayed bridges due to the short life-span of the cables, which suffer hard ambient conditions which can cause rapid deterioration. In fact, cables in 56 bridges in China have had to be replaced up until 2010 [5], which demonstrates the importance of taking advantage of such systems to ensure planning and anticipation.

Finally, SHM systems allow for the creation of accurate models that faithfully reflect the response of mechanical systems to real-life scenarios. The monitoring of structures plays an especially important role in the study of materials, behaviors, forces, etc. The generation of these data sets is really interesting both at the academic level for engineering faculties and research teams and at the professional level for future structural designs.

2.1.3 Application in this project

According to [2] and previously stated by [7], the design of an SHM system consists of 4 step process:

1. Operational evaluation
2. Data acquisition, normalisation and cleaning
3. Feature extraction and information condensation
4. Statistical model development

In the present case, due to the nature of this project, the two parts we are most interested in studying are the first two: *Operational evaluation* and *Data acquisition, normalisation and cleaning*.

For a deeper understanding of the content of these parts, the authors of both papers break these points down as follows:

- Operational evaluation
 - Life/safety and/or economic **justification** of the project
 - Definition of **damage** for this specific structure or system
 - **Conditions** (operational and environmental)
 - **Limitations** on acquiring data

- Data acquisition, normalization and cleansing
 - Acquisition
 - * Methods of measurement
 - * Location of sensors
 - * Hardware used
 - * Storage and/or transmission
 - Normalization
 - * Distinction between environmental variations and damage driven variations
 - * Collection of data for statistical quantification
 - Cleansing
 - * Filtering of signals
 - * Outlier exclusion

The application of these points will be explained in detail in the following pages.

2.2 Energy harvesting

Energy harvesting is known as the process of using the surrounding ambient energy into electrical power [8]. This technique is commonly used for wireless systems, and it is very important in the field of Internet of Things (IoT)

We could interpret this as a small-scale renewable energy generation, as we are taking advantage of the energy present in the surroundings of the system, but using it for only powering a small-scale system.

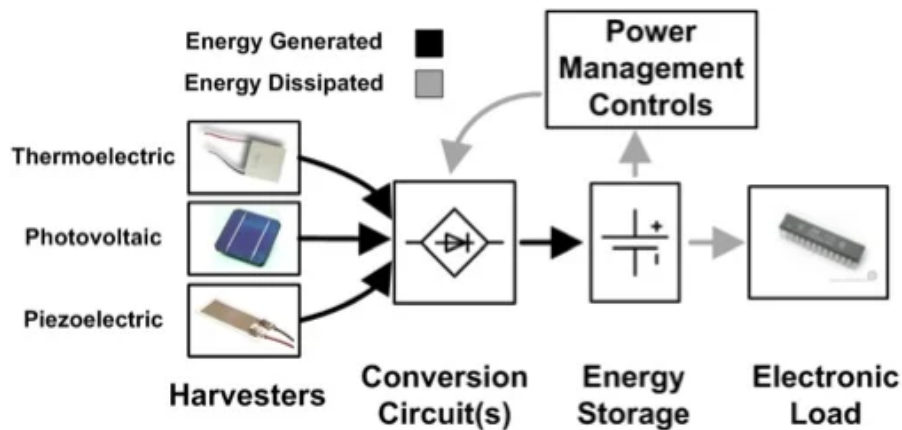


Figure 3: Diagram of Energy Harvesting systems [9]

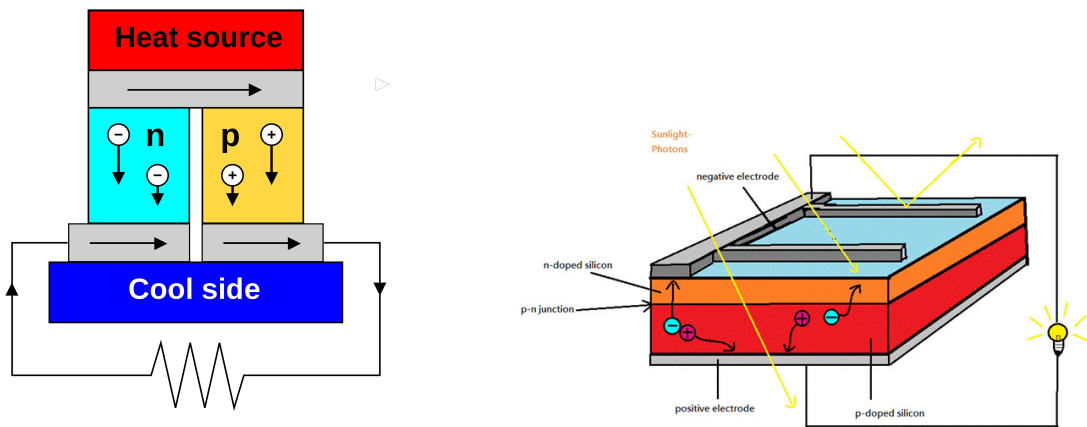
This technique also looks into the replacement of batteries, which have a limited life-span and can be costly regarding to maintenance, while keeping the system independent from the power grid. However, in some cases where the energy source fluctuates or simply disappears for a period of time (like solar energy), small rechargeable batteries can be implemented to ensure the correct operation of the system.

As we will see in the following pages and in the development of this project, the most commonly used environmental energy source in this type of system is solar, but the use of other much less common sources has been studied, which we will explain in the following section.

2.2.1 History and examples

Taking into account the complete definition of Energy Harvesting, we could state that this practice has existed for millennia. Many civilizations used ambient energy to facilitate everyday tasks like, for example, the water mill for grinding wheat grains to obtain flour.

However, we would have to look further on time to observe the first application of Energy Harvesting as we know it nowadays (i.e., the generation of electrical current). Two of the most important events were the discovering of the thermoelectric effect in 1826 and the photovoltaic effect in 1839, although it wasn't until the 1900s that the latter evolved into what we currently know as solar energy with the association of this phenomenon with the quantum theory of light and solid-state physics. [10]



(a) Diagram of a thermoelectric generator

(b) Diagram of a photovoltaic generator

Figure 4: Two of the predecessors of Energy Harvesting

Some examples of the current Energy Harvesting systems are the following [10]:

- Electromagnetic (RF)
- Thermal
- Solar

2.2.2 Benefits

The usage of this procedures can be beneficial for numerous reasons. Energy Harvesting systems allow for independently powered devices, which facilitates their usage in places where the grid is not available or doesn't comply with the minimum standards for the correct operation of these devices.

Moreover, in some applications the connection to the grid can introduce undesired noises and variations in the results of the operations, which makes Energy Harvesting specially interesting for a better isolation from unwanted signals.

This independence from the grid makes many interesting systems possible [10]:

- Wireless Sensor Networks (WSN)
- Solar calculators
- Self-winding watches
- Biomedical implants

2.2.3 Application in this project

In this project we will focus on the solar energy harvesting techniques due to the simplicity of photovoltaic systems and the abundance of this type of ambient energy in the structure's environment.

For this system, a photovoltaic cell will be used.

Photovoltaic Cells

A photovoltaic cell is essentially an electronic device composed by semiconductor materials (normally silicon, although some new materials are currently being researched, like perovskite mineral) that is capable of generating an electric current with light incidence thanks to the photovoltaic effect. This means that, with the incidence of the sun's rays on the surface of the device, the photons are able to excite a flow of electrons that produces the electric current.

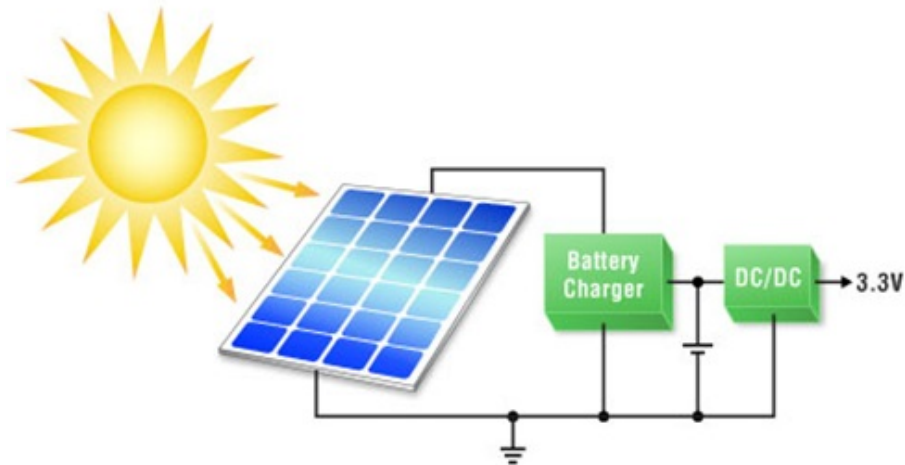


Figure 5: Diagram of a solar cell based EH system [11]

In our case, both the power independence and noise isolation benefits will be taken into account: on the one hand, taking electric power into each and every sensor that will be need to be placed in the bridge can be extremely costly and inefficient; on the other hand, as the bridge is almost entirely made of steel, it will act as an antenna attracting all the noise, so the isolation from the grid will improve noise reduction.

MPPT Control

Maximum Power Point Tracking (MPPT), is a technique used in power electronics that consists on the modification of the electrical working point of a solar panel to ensure that the maximum power is drawn from the photovoltaic system [12].

The MPPT technique is based on the current-voltage graph (I-V), where we can see that the voltage is maintained at an almost-constant value up until a certain current value, where the voltage decreases until it reaches 0V. We can see here in figure 6 how this principle can be observed in a curve:

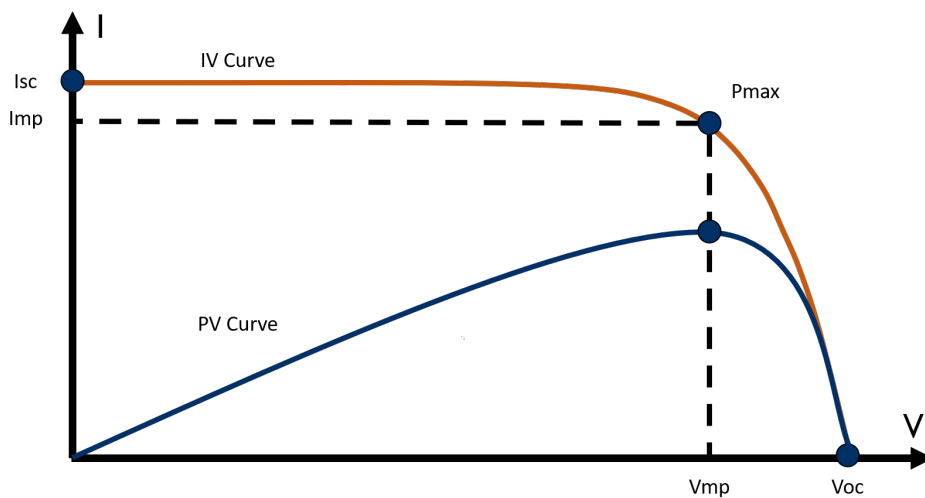


Figure 6: I-V and P curve of a solar panel [13]

As we can see from the curve, by changing the voltage or current of operation of the panels, we can draw a higher power from them, allowing us to fully take advantage of the photovoltaic system.

This method requires the measurement of certain parameters, but usually both voltage and intensity are measured to be digitally processed. With a μ Controller, we can manage the data coming from the sensors and change the DC-DC converter's parameters so as to bring the system as close to the Maximum Power Point as possible.

The MPPT systems currently present in our day to day lives are based on four different methods and algorithms [14]:

- **Perturb and observe method** → The Perturb and Observe method (P&O) is the most widely used method for MPPT, and it consists on the measurement of both voltage and current and its later processing. This method works by changing the output voltage of the PV panel and measuring the resulting I-V values. The system will define the working point when it reaches a maximum point while it's *navigating* through the different current-voltage combinations.
- **Incremental conductance method** → This method consists on the mathematical principle that relates the MP point with the slope of the I-V curve. The algorithm will perform the following relationships [15]:
 - If the **slope is positive**, the maximum power point is located at a higher-voltage position. The system will rise the voltage.
 - If the **slope is negative**, the MPP is located at a lower-voltage position. The system will decrease the voltage.
 - If the **slope is zero**, it means that the system has reached the MPP. The system will stay in this point until otherwise indicated.
- **Current measurement method** → This method is based on the P&O method. However, by assuming constant the voltage of the battery that the system is powering, only the current measurement is needed, which simplifies the installation, although this algorithm has to be thoroughly tested before final implementation because of the voltage assumption. It was introduced by Salas et Al. in [16].
- **Fuzzy logic controller method** → This is one of the most mathematically-complicated methods to implement at first. Nevertheless, it offers a great efficiency. This method has been studied in papers like [17].

Comparing the four methods above, we found that the P&O algorithm is the one that is easier to implement.

Although this system uses more resources because it needs to measure the voltage as well as the current of the PV panel, the operations that the μ Controller needs to perform are easier. The processing unit will only need to multiply both measurements and compare them to the previous one to asses the next steps.

This method, as well as the rest of the ones discussed above, need constant evaluation of the conditions of the circuit, which could take a good amount of the energy produced. For this reason, although the most common approach is to code the algorithm in a μ Controller that manages the switch of a conventional DC-DC converter, we considered that the use of an Integrated Circuit would be more energy-efficient, as well as less space-consuming.

The aforementioned plays in our favor, as most of the commercially available Integrated Circuits that use some kind of MPPT control rely on the P&O algorithm. Moreover, these ICs usually include other interesting functionalities like battery managing or a regulated voltage source.

Although the election of the IC will be explained in the following sections (specifically in section 4.4), it is interesting to face the design of this system knowing that the IC used for power management is the STMicroelectronics SPV1050, which relies on an already embedded MPPT control system.

We can see in the following diagram (figure 7) how this algorithm works:

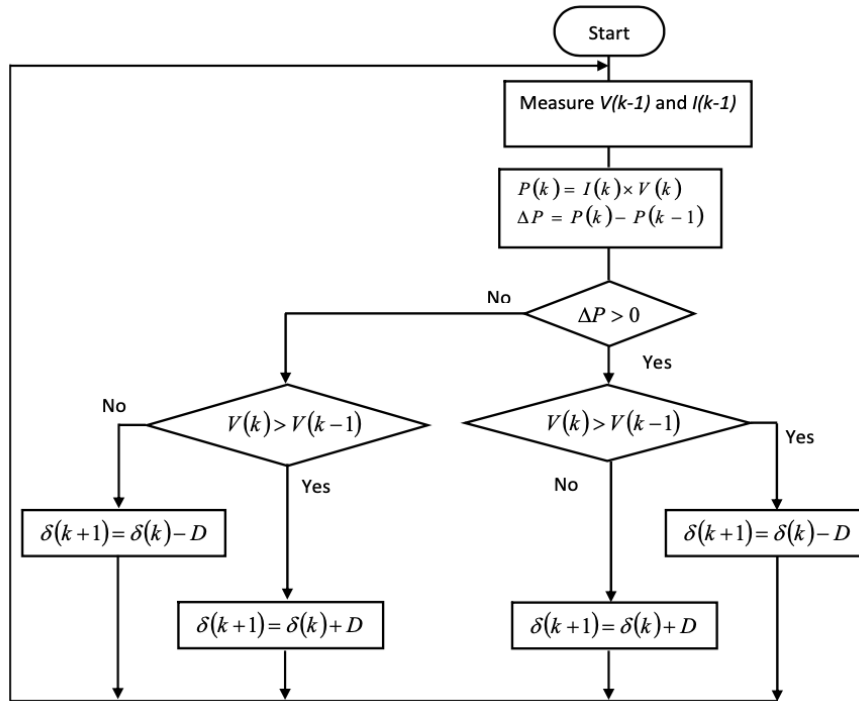


Figure 7: I-V and P curve of a solar panel [13]

Although this will be automatically performed by the Integrated Circuit, it can easily implemented by measuring both the voltage and current at the terminals of the photovoltaic panel with a regular μ Controller or similar.

3 | Needs Assessment

As previously explained, the system that we are designing will be installed on the stay-cables of the *Assut de l'Or* bridge, in Valencia (Spain), which we can see in the following image (figure 8):



Figure 8: View of the bridge in the Arts and Sciences City [18]

The bridge was designed by Spanish architect and structural engineer Santiago Calatrava in the year 2000 and its construction lasted until 2008.

The structure is a cable-stayed bridge with a deck of 160m of span and a variable width of 35 to 39 m, the latter being around the mast. The mast reaches a height of 125m and it holds the deck by means of a 29 stay-cable system arranged in the form of a harp and 4 retaining cables in the back. The weight of this entire structure (taking into account the deck, the mast and the base/pier) is estimated to be around 5600 tons.

The Structural Health Monitoring system that will be designed for this bridge will have to adapt to a pre-existing structure that was not designed to hold this kind of system, which means that some of the dimensions and characteristics of the bridge will have to be looked into and taken into account for the following steps. In the following points, these characteristics will be explained in depth for a better understanding of the choices made in the design of the system.

Furthermore, the system will need to comply with some specifications that will be presented later. Some of these requirements include the independence from the electrical grid, the continuous operation of the system, etc.

3.1 Summary of the structure's specifications

In this section, the crucial dimensions and architecture of the structure will be stated, so as to allow for a better understanding of the measurements to be performed.

3.1.1 Dimensions

As we can see in the diagram below, the bridge has a mast that reaches 118m of height. The mast is connected to the 160m span deck with a group of stay-cables that will be described along the next lines.

On the back of the mast, four 110m restraint cables connect the upper part to the counterweights placed on the south abutment.

For the scope of this project, the measures specified here are, for the most part, of an informative nature.

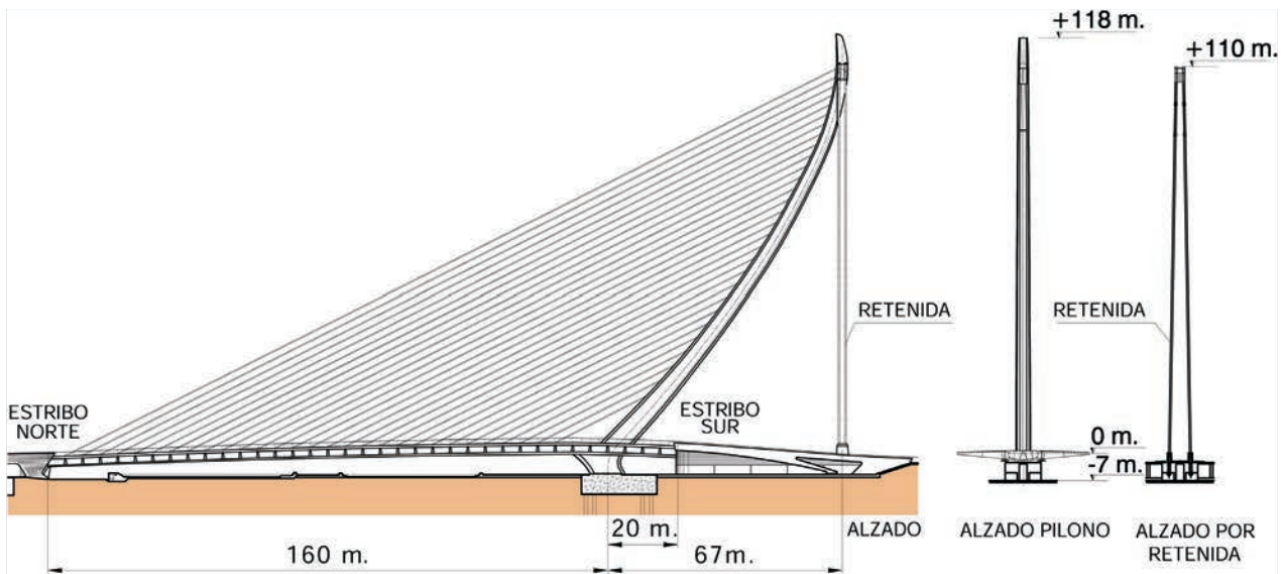


Figure 9: Dimension diagram of the *Assut de l'Or* bridge [19]

3.1.2 Distribution of cables

In this bridge we should differentiate between two groups of cables: the stay-cables and the restraint cables.

Although they are made of the same material and with a similar function, the construction techniques are slightly different, which makes some of the features of the system not applicable to the entire bridge.

Firstly, we have 29 stay-cables that vary on length but are placed at the same angle respect to the horizontal reference and are equidistantly spaced at 5m apart [19]. These cables are

anchored to the deck and the mast of the bridge through the *BBR HiAm Cona* anchorage system.

On the other hand, the retaining cables are attached to the top of the mast at a height of 110m and fall (perpendicularly on the side view and slightly outwards in the front view) towards the south abutment. These cables, together with the weight of the mast, are the ones that compensate for the tension from the stay-cables and, thus, from the weight of the deck.

3.1.3 Architecture of the cables

This is the part that concerns us the most, as the complications of the project come from the differences of design and construction of the cables.

On the one hand, we have the 29 stay-cables, made from **several 0.6" stranded steel cables**. The cables vary in thickness, due to their differences in weight-bearing tensions, and are distributed as follows [19]:

- Cables **1 to 6** → 31 units
- Cables **7 to 20** → 61 units
- Cable **21** → 55 units
- Cable **22** → 49 units
- Cable **23** → 43 units
- Cables **24 to 29** → 31 units

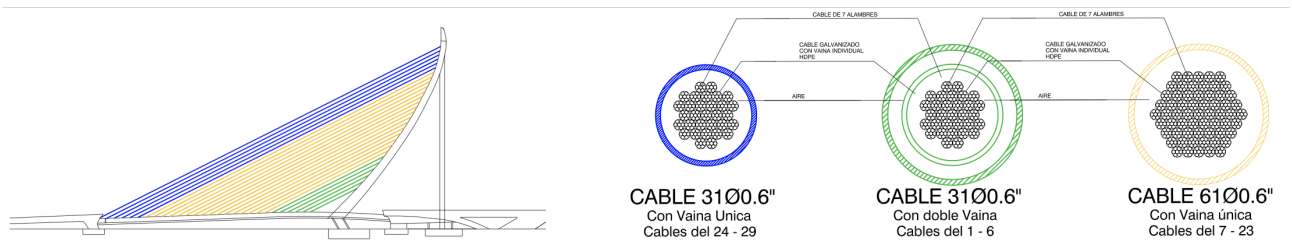


Figure 10: Diagram of the different construction and sheathing of the cables

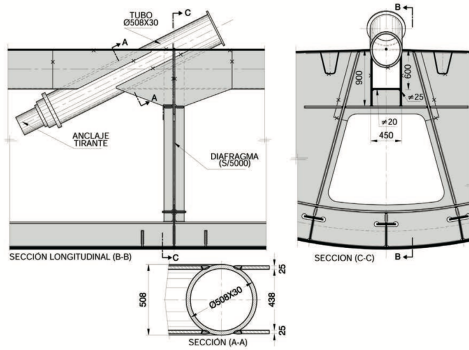
In future pages we will go into more detail on the specifics of the calculations that the diameter differences entail.

On the other hand, however, we do have four retaining cables that have the same specifications. They are all formed by 85 units of 0.6" stranded steel cables [19]. The complication in this part of the bridge is that the retaining cables, as well as the stay cables, are covered by a HDPE sheath. However, the latter is easily accessible, as the cover is not structurally needed, while for the former, the space between the steel cable and the cover was filled with cement grout, making it specially difficult for the installation.

3.1.4 Placement of the system

As a conclusion to these paragraphs in which we have explained the specifications of the structure, in this section we will explain the location of the system in the bridge.

Due to the facility of installation in the stay-cables, this will be the final destination of the system. The sensors will be placed in the lowest part of the cable, due to its accessibility for the installation and future servicing. The cover of the anchorage will provide a strong enough covering for the sensor that will keep it out of reach from the pedestrians.



(a) Diagram of the anchorage of the cables

(b) Dampers of the anchorage installed on site

Figure 11: Details of the sensor location [19]

However, due to the installation of concrete grout fillings on the retaining cables, we will not be able to place any sensor on these, as all the elements on these cables are crucial for the resistance against wind-rain vibrations [19].

3.2 Study of needs and factors to be considered (limitations and conditioning factors)

3.2.1 Precision

For this project precision is a crucial factor, as the changes in the strain of the cables might result on very small changes in the sensor readings. However, this is a regular application of the measuring devices we are going to use, which means that precision should not be a problem while designing this system.

For easier and more efficient readings, the best options will be selected for the sensing device, the amplification section and the processing unit.

3.2.2 Noise rejection ratio

The requirement of a good noise rejection ratio is a standard on electric and electronics engineering projects. However, in this project, the nature of the structure and its geographical placement will play a complicated role on the fulfillment of this specification.

The bridge is almost completely made of steel, which means that, thanks to its large mast and the high quantity of stay cables, it may act as an antenna and collect all electromagnetic noise. This is specially concerning due to the fact that this bridge is located in a highly populated area, which aggravates the presence of noise inducing signals that can hinder the correct measurement of the data.

3.2.3 Independence from the grid

This system will not be connected to the grid for the following reasons:

- **Noise rejection** → Continuing on the noise rejection topic, the independence from the electrical grid will allow for better treatment of these unwanted signals. This is because the grid can induce a 50Hz noise in the circuit, but also because the cables that will have to be installed can also act as antenna for these signals.
- **Cost of installation** → The installation of power cables to all the locations of the bridge might be costly, as the distances traveled by these cables are very long and we need to ensure power stability along the whole system.
- **Energy savings** → The energy savings of making an independent, energy harvesting-based powering system are a key point in the realization of this project. Although the energy consumption of this system will not be high, it constitutes a reason for considering an independent source of power.
- **Difficulty of installation** → The main reason for the design of an grid-independent system is the fact that this bridge is already constructed and it is not prepared to hold a Structural Health Monitoring system. This means that for the installation of power cables, we would need to either alter the aesthetics of the design by adding cables on the outside, or dismantling the majority of the covers of the bridge in order to make a hidden installation while potentially altering some of its structural properties.

3.2.4 Continuous operation

The independence from the grid and specially the power system chosen could lead to possible instability of the power source. This system, however, needs to constantly be connected for the measurements of the bridge.

This means that we will have to implement an energy storage system to this project to store surplus energy for the parts of the day without enough solar power.

3.2.5 Resistance to weather harshness

As this system will have to endure possible weather harshness for many years, the system will have to be protected by a cover.

We can use the cover of the anchorage dampers for storing the components. However, a case can be designed in further updates of the project, in which the PCB and the battery can be stored.

4 | Alternative solutions and justification of the adopted solution

In these following paragraphs, we will explain the different solutions we have considered for the design of this system. Further in this chapter, having explained all the different options, the justification for the solution chosen will be provided.

4.1 Measurement magnitude

In a Structural Health Monitoring system, all the magnitudes that can be measured are interesting. As we previously stated in the explanation of the SHM technique, the sensor systems installed in these structures, apart from ensuring safety of the users and the surroundings, provide a better understanding of their response to normal use and weather inclemency, thus allowing for the creation of mathematical models.

The magnitudes that we found interesting to measure in this bridge were the following:

- **Vibrations** → The measurement of vibrations in the structure, specially in the deck, mast and foundations, allow for an effective way of detecting cracks or even points of possible future failure [20]. The vibration in the cables can also be used to measure their tension [21], although this is a complicated procedure.
- **Strain** → The strain of several structural parts can be measured so as to know the failure points of the bridge. However, the best use for strain measurements is to know the load of the bridge and its distribution along the deck of the bridge.
- **Tension** → The measurement of tension of the cables can also be an interesting magnitude for the SHM system, as the cables are one of the most important elements in a cable-stayed bridge, as they are susceptible to corrosion, fatigue and vibrations [5].

For this project, due to its facility of measurement and its importance for future calculus, **we will use the tension of the cables.**

4.2 Sensor location

For this project, some locations were considered, like the main beams of the deck or the sides of the mast for measuring the strain of the materials. However, as we chose the tension of the cables as our main magnitude to measure, the options for placing the sensor are reduced.

As the sensor has to be attached to the cable, we can place it in almost every part. However, in terms of accessibility, the lowest part of the cable is the best one. This part holds the damper and anchorage of the cables to the deck, which makes for a very accessible placement for installation and future maintenance.

We can see in the following image (figure 12) where the sensor will be placed:

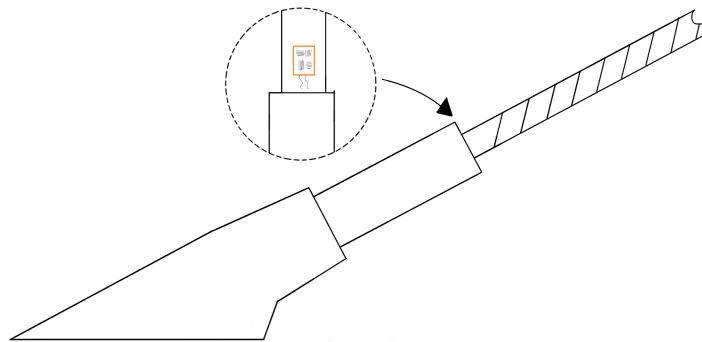


Figure 12: Sketch of the placement of the sensor in the anchorage

4.3 Type of sensor

There are many ways in which we can measure the tension of the cables. As we previously explained, we can use the vibrations of the cable to estimate the tension. We can also use strain gauges for this measurement. These are the different types of sensors that were considered for this purpose:

- **Accelerometer** → An accelerometer is a sensor that can measure the acceleration (the change in velocity) of a body [22]. In our case, this sensor could be used for measuring the frequency at which the cables oscillate with the wind or other natural forces and, as previously explained, estimate the tension.
- **Vibrating Wire Strain Gauge** → A Vibrating Wire Strain Gauge (VWSG) is a gauge that has a cable on the inside. This cable needs to be excited with an electric pulse, and the response of this cable is to be measured. This is almost the same operation as the accelerometer, but in a small scale. This sensor can be welded to steel cables, as we can see in figure 13, but it also can be used in other steel or concrete pieces.
- **Film Strain Gauge** → A film Strain Gauge is one of the most well-known sensors in this kind of applications. It consists of a thin conducting cable folded in a zig-zag pattern inside of an insulating protecting film. This is an interesting sensor due to the simplicity of its operation and installation and the little space they occupy.

The accelerometer option, although innovative, is a complicated solution to implement, as a powerful processing unit is needed in order to determine the frequency of vibration and calculate the tension.

On the other side, the VWSG was a good option in terms of implementation. Unfortunately, the size of this sensor, which we can see in the image below, is too big for the implementation in this application.



Figure 13: A Vibrating Wire Strain Gauge installed on a steel rod

Finally, we chose a **film Strain Gauge** for this application. We considered it is a great sensor due to its simplicity and the convenience of its signal conditioning. Also, its reduced size makes the installation on these cables possible, as we saw on a previous diagram that the space between the steel and the protective cover is reduced. We will now explain what a strain gauge, how its application to this project needs to be done, and how it is going to help us measure the tension of the cables.

4.3.1 Strain Gauge and its application

Definition and operation

A Strain Gauge (SG) is a sensor formed by a thin conducting foil inside an insulating film. This sensor detects the mechanical strain of the point of the material it is attached to and translates it to a change in its resistance [23]. In the following image, figure 14, we can see all the parts herein mentioned.

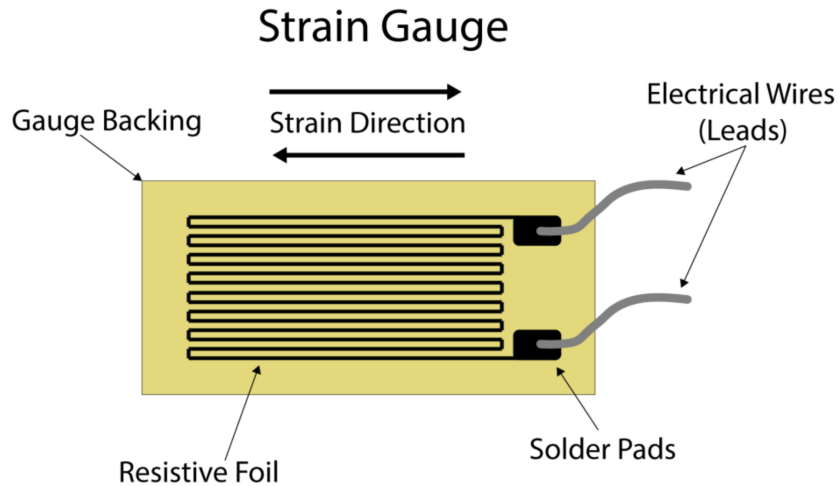


Figure 14: Diagram of a film strain gauge [24]

The Strain gauge is based on the physical principle that defines the electrical resistance of a conductor according to its cross section, length and conductivity. This relationship is defined as follows:

$$R = \frac{\sigma \cdot L}{A} \quad (4.1)$$

Where:

- R → resistance of the conductor (in ohms, Ω)
- σ → resistivity of the material (in ohms/meter, Ω/m)
- L → length of the conductor (in meters, m)
- A → area of the section of the conductor (in meters squared, m^2)

With this expression, we can better understand that, when the material to be measured, and thus, the sensor, is put under stress, the elongation of the conductive material in the strain gauge and its consequent reduction in cross-sectional area, will produce an increase in the sensor's resistance.

This change in its internal resistance will be reflected in a change of output voltage on the Wheatstone Bridge that it will be connected to [23].

For this element, various models were considered. Amongst them, a Strain Gauge by the company HBM (model 1-VY41-3/350). However, as we can see in the following image (figure 15), the disposition and inclination of the measuring grids was complicated to install in the bridge.

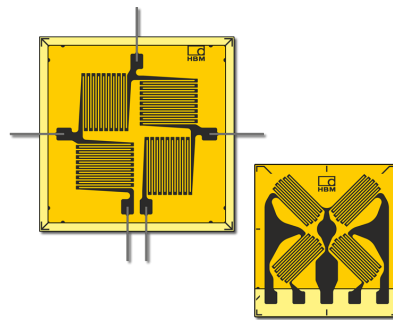


Figure 15: Diagram of the HBM Full-Bridge Strain Gauges

Finally, the model chosen for this project was the **OMEGA SGT-3G/350-FB41**, which we can see hereunder in figure 16. This strain gauge has a nominal resistance of 350Ω .

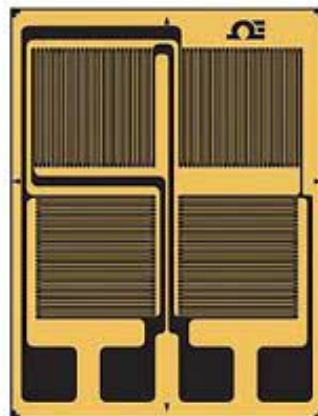


Figure 16: Diagram of the OMEGA SGT-3G/350-FB41 Strain Gauge

Below, we will explain two concepts behind the implementation of these gauges in the project.

Wheatstone bridge

In this paragraph, we will briefly explain what a Wheatstone bridge is and how it is necessary for the application of our sensor, the strain gauge.

Wheatstone bridges are one of the most elemental and useful tools in the industry. Typically, a Wheatstone bridge consists of four strain gauges, although a half-bridge can be created using only two strain gauges [25], and they usually come represented as figure 17 shows.

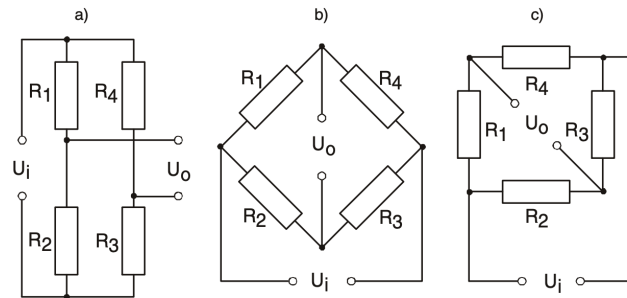


Figure 17: Wheatstone bridge representations: a) rectangular, b) rhomboidal, c) square [25]

An advantage of this kind of bridge is that it delivers a linear response. Moreover, the readings are compensated against temperature-induced strain variations, which means that, even though our system will be placed outdoors, the temperature changes will not affect the tension read-outs of the sensor [25]. This result is usually obtained by performing the "dummy gauge" technique, which we will explain hereunder.

Dummy gauge technique

The dummy gauge technique is an extensively used procedure in the measurement of strain in order to compensate for the temperature-induced strain variations. It consists of an extra strain gauge placed in a material with a similar thermal behavior as the one we are measuring. In other cases, however, this strain gauge can be placed perpendicular to the measured strain, which prevents the measurement of this magnitude while allowing for the thermal expansion or contraction forces to be perceived, as we can see represented in the following image, figure 18.

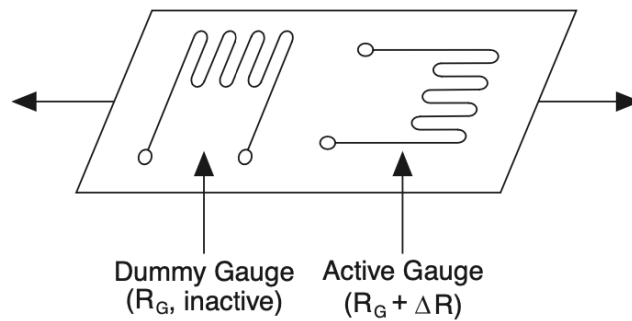


Figure 18: Dummy gauge in perpendicular configuration for temperature compensation [26]

This technique, applied in a Wheatstone bridge, allows for an balanced variation of the resistance of the strain gauges, which thanks to the counterbalance generated by the two branches of the bridge, cancels the voltage variation out and allows for a reading without thermal errors.

In addition, [23] recommended their use, as they indicate in the following paragraph:

Experience from taking measurements shows that dummy gauges should be used in the bridge circuit if measurements are made at varying temperatures and if circumstances permit it. There are two reasons for this recommendation:

1. *The thermal expansion coefficient of the measurement object material can vary by a relatively large amount and may deviate from values upon which the manufacture of the temperature compensated strain gauges are based.*
2. *With larger temperature variations during the measurement the spread in the temperature responses of the strain gauges within a production lot is substantially smaller than the temperature dependent changes in resistance that still occur in spite of the matching that has been undertaken.*

(Stephen Keil, 2017 [23])

4.4 Power managing

For the managing of the power circuit some options were considered: a digitally controlled DC-DC converter was the main solution to be implemented, as it is one of the most common circuits for this kind of applications.

This solution, however, was a more complex application. It added calculation time and it would not have been as electrically efficient as we desired for this project. Moreover, the space occupied by a custom system would have been considerably larger than an Integrated Circuit option.

For these reasons, we decided that the best option for this project was to implement an Integrated Circuit that could handle the conversion of the energy from the panel and the

storage in a battery. In this category of components, different models were considered, which we can see in the following table:

Comparison between Power IC models			
Specifications	SPV1050	SPV1040	TPS612994
Input voltage range	150mV - 18V	0.3V - 5.5V	0.5V - 5.5V
Input current range	30 μ A min	-	120mA
Output voltage range	2.2V - 5.3V	2V - 5.2V	1.8V - 5.5V
Output current range	up to 70mA	1.8A (inductor)	0 - 200mA
Protection systems	Undervoltage Overvoltage	Overcurrent Overtemperature	Thermal
Conversion modes	Buck Buck-Boost	Boost	Boost
Regulated sources	3.3V 1.8V	NONE	NONE
Other characteristics	MPPT integrated	MPPT Integrated	-

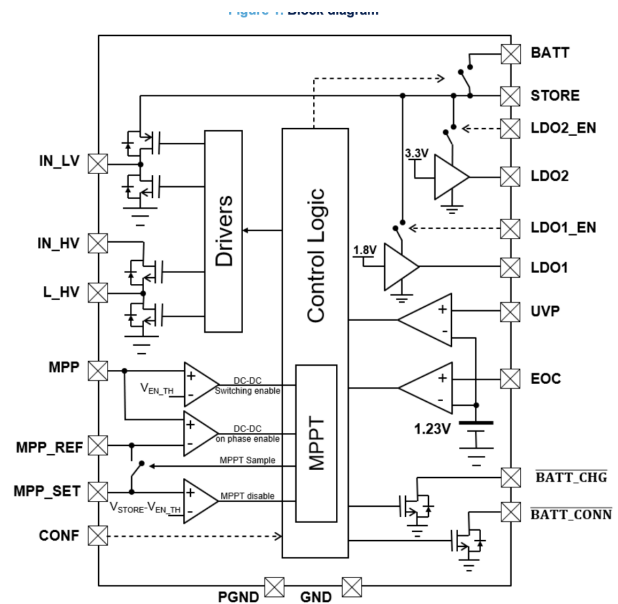
Table 4.1: Comparison between three Power IC models

Finally, the model chosen was the SPV1050 for its specifications and, specially, for both having an MPPT controlled converter and for having a regulated 3.3V source that will be used for the ESP32 μ Controller. Moreover, as this Integrated Circuit is designed to be a battery charger, it has some protection systems that will help to maintain it in good charge condition.

In the following images, we can see the chip (image 19a) and its internal structure (image 19b):



(a) Image of the IC



(b) Block diagram of the IC

Figure 19: STMicroelectronics SPV1050 Integrated Circuit (from datasheet)

We also extracted a section of the characteristics table from the datahsheet, which we can

see in the following image:

Symbol	Parameter	Test conditions	Min.	Typ.	Max.	Unit
Load/battery operating range						
I _{BATT}	Output current to load/ battery	boost configuration	-	-	70	mA
		buck-boost configuration	30	-	-	
V _{BATT}	BATT pin voltage range		2.2	-	5.3	V
R _{BATT}	Pass transistor resistance	BATT_CONN = low	6	7	8	Ω
Bandgap						
V _{BG}	Internal reference voltage		-	1.23	-	V
	Accuracy		-1	-	+1	%
UVP						
V _{STORE(UVP)}	V _{STORE} undervoltage protection range	$(V_{UVP} + UVP_{HYS}) < (V_{EOC} - EOC_{HYS})$	2.2	-	3.6	V
UVP _{HYS}	UVP hysteresis	V _{STORE} rising	-	5	-	%
EOC						
V _{STORE(EOC)}	V _{STORE} end-of-charge voltage range	$(V_{UVP} + UVP_{HYS}) < (V_{EOC} - EOC_{HYS})$	2.6	-	5.3	V
EOC _{HYS}	EOC hysteresis	V _{STORE} falling	-	-1	-	%
STORE						
V _{STORE}	STORE pin voltage operating range		V _{STORE(UVP)}	-	V _{STORE(EOC)}	V

Figure 20: Specifications table from SPV1050's datasheet

5 | Detailed description of the solution adopted

In this chapter we will discuss in depth the explanations of each part, the calculations, the results, etc. The explanation will be divided in various sections according to the stages of the system (sensing, conditioning, processing, etc.) which will allow for a better understanding of the design.

5.1 Measurement magnitude

As we previously stated, the magnitude we will be measuring will be the tension of the cables.

The way we will be doing this is by measuring the changes of resistance in the sensor and comparing them to the values of the bridge without any load. Firstly, nonetheless, we need to know what is the value of the tension of the cables without any load.

In the technical documentation of the bridge, published in the report [19], little to no information about the tension of the bridge in the construction is provided. In spite of this, as we saw earlier in this report, many other physical characteristics of the bridge are available.

The tension of the cables, however, is a parameter that, should it had to be calculated, would be completely outside the scope of this project, which is focused on electronic design. For this reason, in order to design the system, some assumptions have been carried out (all of them backed by the professors at the department of Civil Engineering of the Polytechnic University of València (UPV)).

The approximations are the following:

- The maximum tension that the cable system can support is around 300 MPa. This is the maximum mechanical tension that the anchorage system previously mentioned can support [19], and it will be taken into account due to the fact that structural cable steel can endure tensile forces around 1770 MPa or more [27].
- We will consider that the cables of this bridge were prestressed to a 20% of this maximum tension, which is a good safety margin to design the system with.
- This tensile strength is about 60 MPa, which leaves us a margin to measure the increase of this magnitude once traffic flows over the bridge and also to measure a possible decrease in the tension, which would indicate a possible failure of the anchorage system or of the cable.

In case the calculations of the length and section of the cables are necessary to obtain the force acting in them, we approximated them by using image 9 in *AutoCAD*. We can see their value in the following table:

Cable measurements			
Num	Length (in m)	Number of 0.6" cables	Section (cm ²)
1	29	31	232
2	40	31	232
3	48	31	232
4	60	31	232
5	72	31	232
6	81	31	232
7	91	61	456
8	100	61	456
9	109	61	456
10	115	61	456
11	123	61	456
12	130	61	456
13	140	61	456
14	157	61	456
15	154	61	456
16	162	61	456
17	169	61	456
18	178	61	456
19	185	61	456
20	192	61	456
21	200	55	411
22	208	49	366
23	214	43	321
24	219	31	232
25	227	31	232
26	233	31	232
27	241	31	232
28	246	31	232
29	250	31	232

Table 5.1: Dimensions of the cables for further calculations

These data, although not useful for the safety application of the system, it can be interesting for further academic applications (e.g.: mathematical models of the structure).

As we previously stated, the system will be based on a sensor that will measure the tension force on the stay-cables of the bridge. The device in charge of this task will be a strain gauge, the operation, specifications and implementation of which will be explained in the following paragraphs.

5.2 Signal conditioning

In this first section of the system, the necessary signal conditioning stages will be implemented in order to feed the micro-controller with a suitable voltage range for its Analog to Digital Converter (ADC).

All of the following calculations have been carried out taking into account that the power supply of the system allows for a maximum of 3.3V (stemming from the photovoltaic battery-charging IC that will be hereafter explained). This means that the Instrumentation Amplifier, as well as the Operational Amplifiers (Op Amp), will need to have an offset voltage to compensate the asymmetry of this power supply.

The section includes:

- An **Instrumentation Amplifier (Inst Amp)** that will convert the differential signal from the strain gauge to a single-ended one, as well as provide a voltage gain and an offset.
- A **Low Pass Filter (LPF)** that will eliminate the unwanted frequencies from the system as well as provide a voltage gain.
- A **Subtractor** that will eliminate the offset added in the Inst Amp stage so as to bring the signal back to a 0V to 3.3V range signal.

5.2.1 Instrumentation Bridge: adaptation of signal voltage range

In order to continue with the calculations of the component values that will be used to condition the signal, we need to know what is the range of voltages we need to expect at the strain gauge output. In this way, we can calculate how much gain the following stages (Inst Amp and LPF) will need to have. For this purpose, the calculations explained below have been performed (all taking into account the topology indicated in figure 21 hereafter):

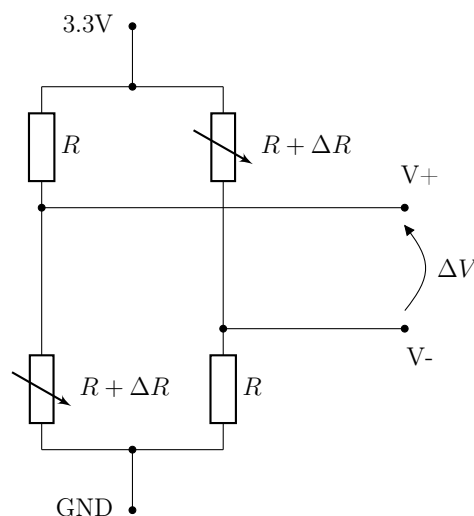


Figure 21: Instrumentation bridge used in the project

Firstly, having in mind the range of tension forces we assumed previously (60 MPa for the prestressing and 300 MPa of absolute maximum tensile strain) we calculated the elongation of the cable for two cases:

- 0 MPa, which will be the value of a unstressed cable (decrease of 60 MPa, in our case)
- 300 MPa, which will be the maximum stress the cable system will endure before its complete failure.

The following equation (Hooke's law) was used to calculate the elongation of the cable:

$$\epsilon = \frac{s}{E} \quad (5.1)$$

where:

- ϵ → Elongation of the material (in meters per meter (m/m), but usually expressed in micrometers per meter ($\mu\text{m}/\text{m}$))
- s → Strain of the material (in Pascals (Pa))
- E → Young's modulus (assumed 200 GPa for this material)

The maximum stressing of the cable (a variation of +240 MPa) is:

$$\epsilon_1 = \frac{240 \cdot 10^6}{200 \cdot 10^9} = +1200 \mu\text{m}/\text{m} \quad (5.2)$$

For the de-stressing of the cable (a variation of -60 MPa) we obtained:

In the same way, for the de-stressing of the cable (a variation of -60 MPa) we obtained:

$$\epsilon_2 = \frac{60 \cdot 10^6}{200 \cdot 10^9} = -300 \mu\text{m}/\text{m} \quad (5.3)$$

For the first value, however, we proceeded with a **+1300 $\mu\text{m}/\text{m}$** to compensate for the approximations that were previously carried in the strain limitations of the bridge.

Knowing these values, we can now calculate the variation in the resistance of the strain gauges. For this, we used the following equation:

$$\Delta R = R_n \cdot k \cdot \epsilon \quad (5.4)$$

where:

- ΔR → Variation of the Strain Gauge's resistance
- R_n → Nominal resistance of the SG (350 Ω in this case)
- k → SG factor (assumed 2 for almost all SGs in the market)
- ϵ → Elongation of the material under the SG.

For the elongation values previously obtained, we calculated the following variations in resistance:

$$\Delta R1 = 350 \cdot 2 \cdot 1300 = +0.91\Omega \quad (5.5)$$

$$\Delta R2 = 350 \cdot 2 \cdot (-300) = -0.21\Omega \quad (5.6)$$

Finally, once we have these data, we can calculate the variation of differential voltage of the SG. Knowing that the SGs are arranged in a full-bridge configuration but only two of them are reactive to the axial strain of the cables, we can use the following equation:

$$\Delta V = V_{sup} \cdot \frac{\Delta R}{2 \cdot R_n + \Delta R} \quad (5.7)$$

were:

- ΔV → Variation of the differential voltage
- V_{sup} Supply voltage (3.3 V in our case)
- ΔR → Variation of the SG's resistance
- R_n → Nominal resistance of the SG (350 Ω in this case)

Substituting our resistance variation values previously calculated, we obtain the following voltage deviations:

$$\Delta V1 = 3.3 \cdot \frac{0.91}{2 \cdot 350 + 0.91} = 4.28mV \quad (5.8)$$

$$\Delta V2 = 3.3 \cdot \frac{-0.21}{2 \cdot 350 - 0.21} = -990.30\mu V \quad (5.9)$$

As we can see on the values calculated, the measurements of the sensor will not be symmetrical, that is why we will perform the next calculations to obtain the value of the gain of the system:

First, we calculate the complete variation of the voltage:

$$\Delta V = \Delta V_1 - \Delta V_2 = 4.28 \cdot 10^{-3} - (-990.30 \cdot 10^{-6}) = 5.27mV \quad (5.10)$$

We need the range of this signal to be between 0V and 3.3V, so we calculate the gain according to those parameters:

$$Gain = \frac{\Delta V_{out}}{\Delta V_{in}} \quad (5.11)$$

where:

- ΔV_{out} → Range of the signal voltage after the conditioning stage.
- ΔV_{in} → Range of the signal voltage before the conditioning stage.

In our case, for a $[0 - 3.3]V$ signal, we will obtain the following value for the gain:

$$Gain = \frac{3.3}{5.27 \cdot 10^{-3}} = 625.63V/V \quad (5.12)$$

In our case, we found that the most accurate division of the gain between the two stages using E24 normalized resistors and E12 normalized capacitors is the following:

- **Inst Amp** : 8.66 V/V
- **LPF** : 72.25 V/V

In the following sections, the distribution of this gain will be further analyzed.

5.2.2 Instrumentation amplifier

For this first stage of the signal conditioning of the sensor, we chose the INA333, by Texas Instruments.

Gain of the stage

As stated in the datasheet, the resistor that will determine the gain of the system will be calculated as follows:

$$R_g = \frac{100 \cdot 10^3}{Gain - 1} \quad (5.13)$$

By substituting the gain value for the one we need to reach, we obtain the following resistor value:

$$R_g = \frac{100 \cdot 10^3}{8.66 - 1} = 13.06 \cdot 10^4 \quad (5.14)$$

The most appropriate E24 normalized value that we found is 13k Ω

With this normalized value, we will obtain a gain:

$$Gain_{1-Norm} = 1 + \frac{100 \cdot 10^3}{(13 \cdot 10^3)} = 8.69V/V \quad (5.15)$$

Reference voltage

Firstly, we have to take into account that the signal received by the Inst Amp has a range between -990.3 μ V and 4.28mV and the ADC of our μ Controller *reads* values between 0V and 3.3V, which means that the negative part of the input voltage will have to fit into the [0 – 3.3]V range.

With this end in mind, we will need to add a reference voltage to the Inst Amp that will rise the -990.3 μ V to be 0V. This can be calculated as follows:

$$V_{ref} = -\Delta V_{min} \cdot Gain \quad (5.16)$$

where:

- **V_{ref}** → Reference voltage to be applied to the Inst Amp
- **ΔV_{min}** Lowest voltage of the range (or most negative).
- **Gain** → Gain of the entire conditioning system

$$V_{ref} = -(-990.3 \cdot 10^{-6}) \cdot 625.63 = 619.55mV \quad (5.17)$$

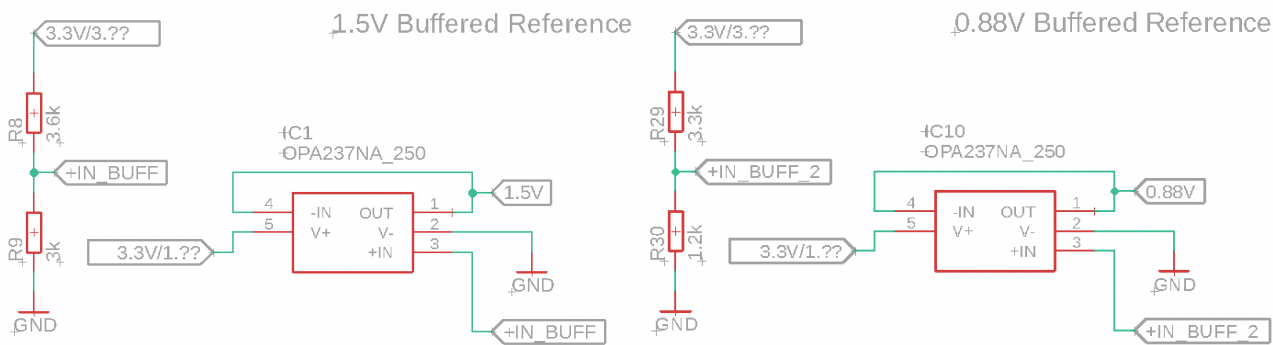
This, however, is not the only reference voltage that will have to be accounted for. As we explained previously, this system will be powered by a low voltage source (3.3V), which means that the operational amplifiers will have a non-symmetrical power source. In order to solve this, a 1.5V reference will be provided for these stages in order to *simulate* a symmetrical rail-to-rail power source.

The problem that arises from this is that the signal will be cut-off if it arrives to one of the limits (0V or 3.3V), which means that we will have to rethink the reference voltage. We will do this, instead of rising the voltage of the signal to match the [0 – 3.3]V range, by lowering the signal so that the range can oscillate symmetrically along the *reference axis* (0V).

As we can see, as the Op Amps have a 1.5V reference, our former *reference axis*, which was situated at 0V, is now located at the 1.5V mark. This will be implemented from the beginning in the Inst Amp by combining both reference voltages, so our final reference voltage will be:

$$V_{ref-2} = 1.5 - V_{ref} = 1.5 - 619.55 \cdot 10^{-3} = 0.88V \quad (5.18)$$

This will be implemented by using voltage dividers, as we can see in the following schematics from the **Eagle** PCB-designing software (figures 22a and 22b):



(a) 1.5V Reference

(b) 0.88V Reference

Figure 22: Schematic diagrams of the references in *Eagle*

We can also see in the following image (figure 23) how the Instrumental Amplifier has been implemented in *Eagle*. The tags connected to the pins of the Integrated Circuit are representations of connections between other parts of the PCB (e.g.: V+ and V- are the connections of the Strain Gauge, and V_Inst, the output of the amplifier).

Instrumentation Amplifier

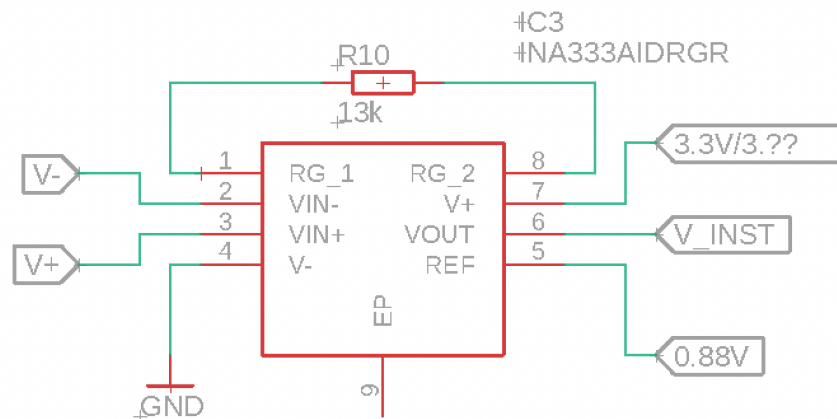


Figure 23: Schematic diagram of the Instrumentation Amplifier in *Eagle*

5.2.3 Low-pass filter

For this section, the Texas Instruments *Filter Design Tool*. This software allows for a precise calculation of the components of the filter while maintaining as accurately as possible the specifications of the system. In our case, the filter was obtained by tuning the following parameters:

- **Gain** → 67.00 V/V
- **Cut-off frequency** → 30Hz
- **Order** → 4th order
- **Response** → Butterworth
- **Topology** → Sallen-Key
- **Component normalization**
 - Resistors: E24 (5%)
 - Capacitors: E12 (10%)

We obtained a two-stage filter with a gain of 8.5 V/V each one, which comes to an overall gain of 72.25 V/V. We can see the topology of the filter in the image below, figure 24:

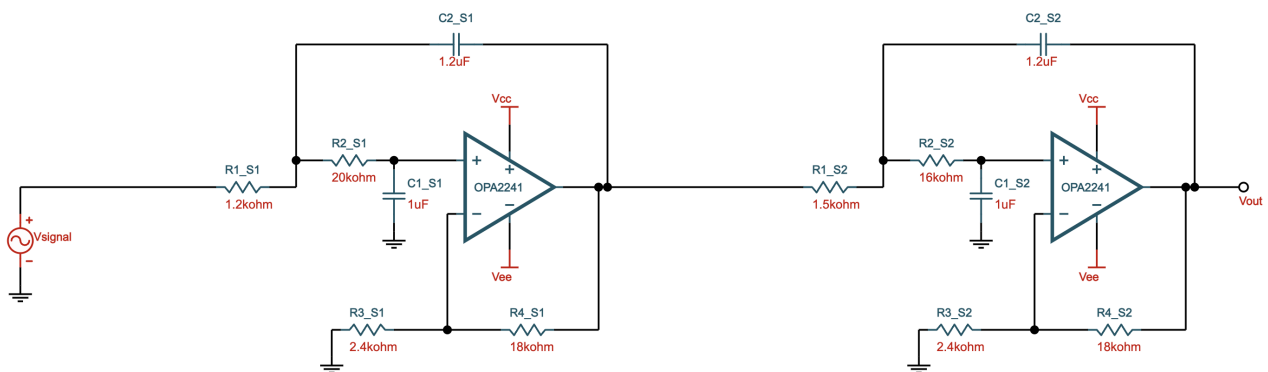
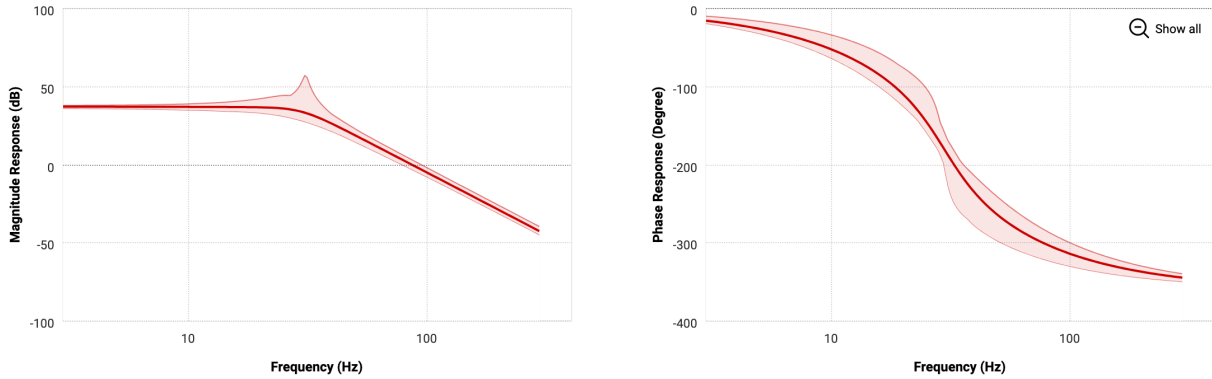


Figure 24: Schematic diagram of the LPF designed in the Texas Instruments suite

In the following Bode Diagrams, we can see the response in magnitude (figure 25a) and phase (figure 25b) response to a spectrum of frequencies including the $[10 - 100]Hz$ decade and the 30Hz cutoff frequency:



(a) Magnitude diagram of the LPF

(b) Phase diagram of the LPF

Figure 25: Bode Diagrams of the system

In the next image (figure 26), the implementation in *Eagle* is shown. As well as in the Instrumental Amplifier, the connections between the different parts of the circuit have been represented with tags (e.g.: V_Inst is the input of the filter, and OUT_B is the conditioned output).

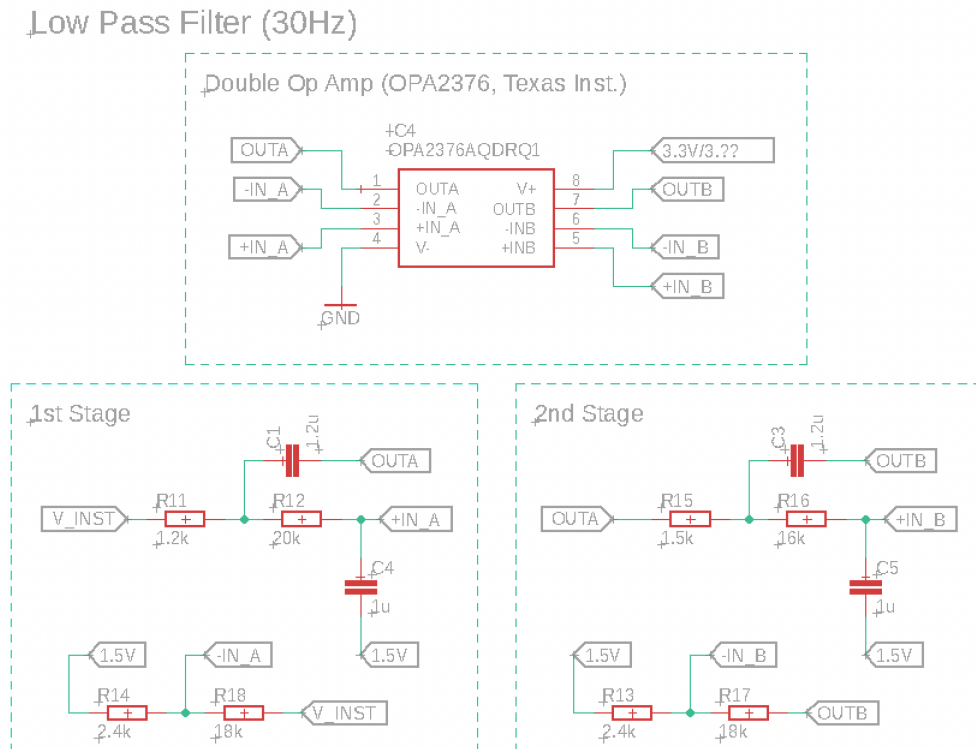


Figure 26: Schematic diagram of the LPF in *Eagle*

5.2.4 Subtraction of the 1.5V reference

Once we have conditioned the signal to fulfill the voltage range requirement, we have to subtract the 1.5V offset, as the resulting signal from the Inst Amp and the LPF exits this stage with this voltage as a reference point.

In order to do this, a subtraction circuit has been designed. For this purpose, we used an Op Amp configured to have a unit gain (so as to not modify the voltage range of the resulting signal). To this Op Amp's non-inverting input, the conditioned signal will be connected, leaving the 1.5V reference from the voltage divider to the inverting input. We can see in figure 27 how this circuit is constructed:

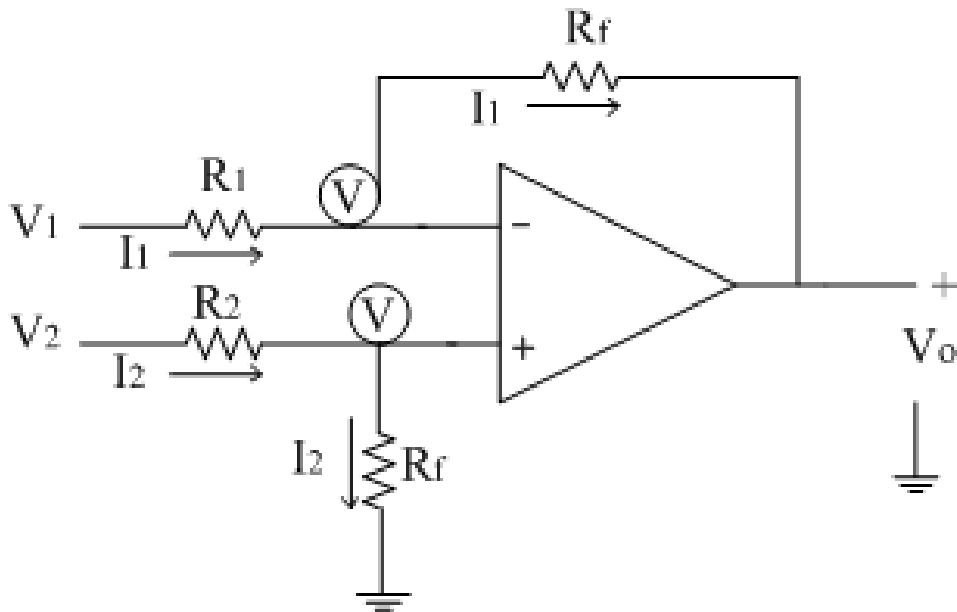


Figure 27: Schematic diagram of the subtractor circuit

This circuit's transfer function looks as follows:

$$V_o = \left(1 + \frac{R_f}{R_1}\right) \cdot \left(\frac{R_f}{R_2 + R_f}\right) \cdot V_2 - \frac{R_f}{R_2} \cdot V_1 \quad (5.19)$$

In our case, given that we need unit gain, we will assume that $R_f = R_1 = R_2$, which means that the transfer function will simply look as follows:

$$V_o = V_2 - V_1 \quad (5.20)$$

This stage of the conditioning section has been implemented as figure 28 shows:

Offset subtractor

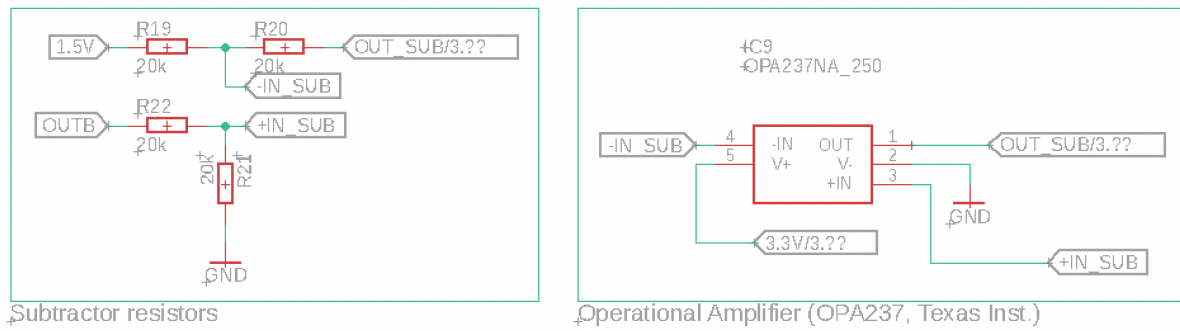


Figure 28: Schematic diagram of the offset subtractor in *Eagle*

5.3 Processing of the signal

For the processing of the signal, an ESP32 μ Controller will be used. This controller will be added to the system's Printed Circuit Board (PCB) and will analyze the signal exiting from the conditioning stage.

The main points of the implementation of this controller are the programming method (USB-UART) and the utilization of the systems available in the controller (the Analog to Digital Converter (ADC) in our case). These two sections will be explained hereunder.

5.3.1 Programming the μ Controller

For programming the ESP32, an USB-UART converter has been implemented. This circuitry will allow us to install the small programs that will manage the communications of the board and, of course, the processing of the signal. For the correct operation of this circuit, a USB isolator has also been implemented.

We can see in the images below (figure 29 and 30) how this stage of the circuit has been implemented in **Eagle**:

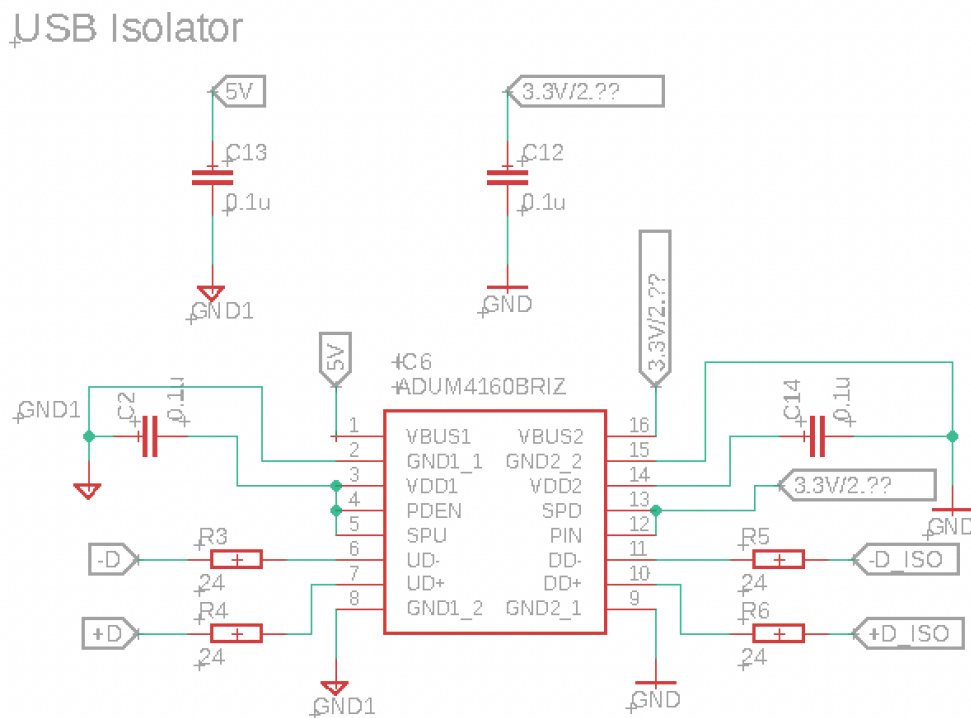


Figure 29: Schematic diagram of the USB isolator in *Eagle*

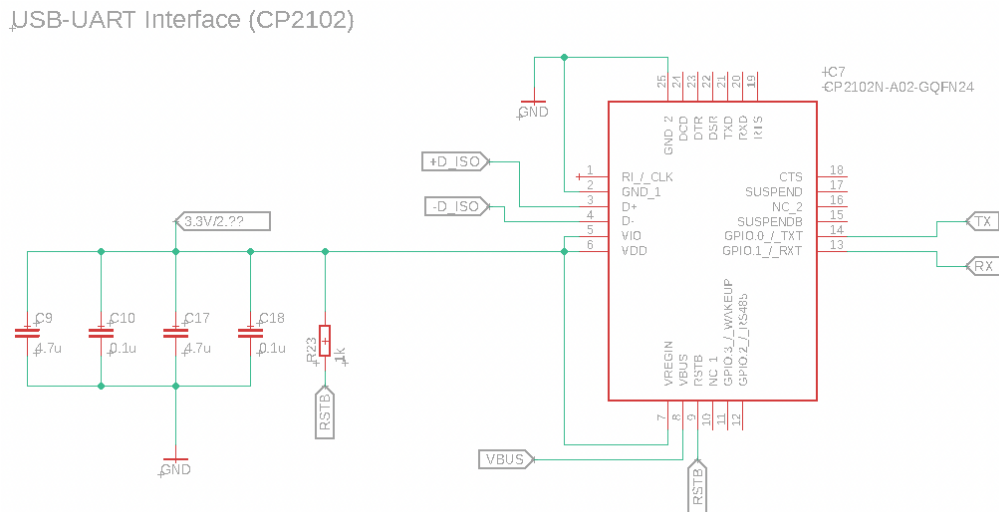


Figure 30: Schematic diagram of the UART interface in *Eagle*

5.3.2 Analog to Digital Converter

The signal extracted from the sensor and conditioned in the previous stages of the circuit will enter the ESP32 μ Controller via one of the ADC pins, in which the analog signal will be converted into digital values that can be processed.

This ADC has the following characteristics:

- **Signal Range** \rightarrow 0V to 3.3V
- **Resolution (bits)** \rightarrow 12 bits
- **Digital Range** \rightarrow 0 to 4096 (2^{12})

5.4 Power Source

In this section, we will address one of the main points of this project, which is the power source of the system.

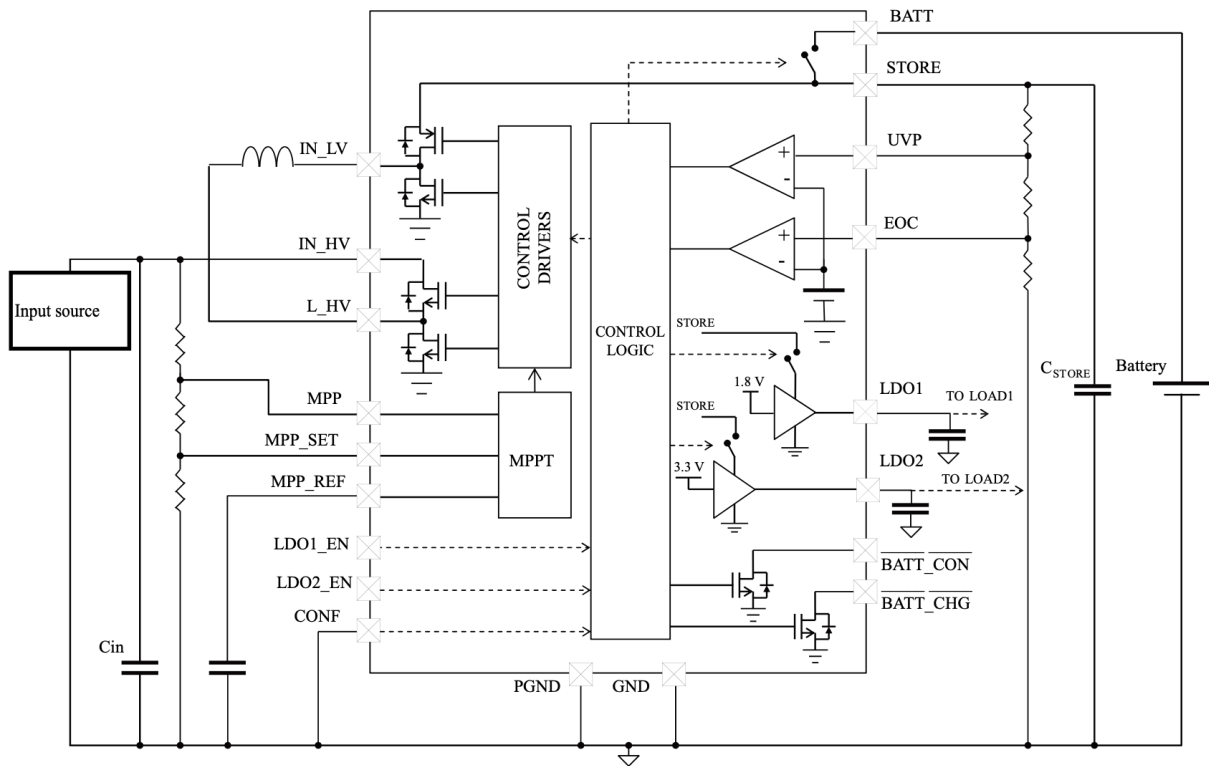
As we previously stated in the background knowledge chapter (chapter 2), this project will be based on the *Energy Harvesting* concept, which essentially means that our power source will take advantage of the ambient energy so as to provide electrical energy to the circuits. In our case, this will consist of a photovoltaic panel (subsubsection 2.2.3), which will harness the solar energy present in the location of the bridge; a DC-DC converter, which will transform the energy harvested to a usable source; and a battery, which will ensure the correct operation of the system when no solar energy is available (e.g.: at night or with cloudy skies).

As the choice of the components of this stage have been previously explained by using table 4.1, we will focus on the calculations of the passive components of the DC-DC converter.

5.4.1 DC-DC Converter

For this power source, the SPV1050 Integrated Circuit (IC) was utilized. This is a low-voltage, low-power integrated DC-DC converter with an option for MPPT control and a charging port for batteries.

The regular application of this IC in buck-boost mode looks as indicated by figure 31:



AM03399

Figure 31: Regular buck-boost application of the SPV1050

The calculations performed will be thoroughly explained along the next paragraphs.

Battery management

Firstly, we will calculate the part of the IC dedicated to controlling the battery charge. This part consists of 3 resistors and one capacitor, as we can see in the following image (figure 32):

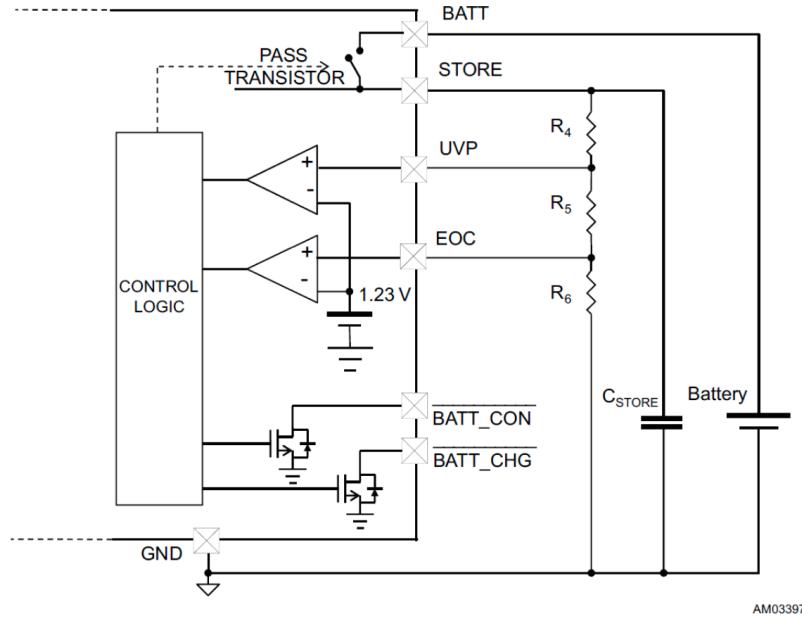


Figure 32: Close-up view of the components in the battery management section

First, we need to set a value for the total output resistance ($R_{OUT(TOT)}$, which is the series combination of the three resistors in the image (R_4 , R_5 and R_6)). For this total resistance, a value of $12.8 \text{ M}\Omega$ was selected. This is the value that, once applied to normalized resistors, comes close to an accurate distribution of resistors. This value also fulfills the datasheet's requirement that $R_{OUT(TOT)}$ has to be selected between $10 \text{ M}\Omega$ and $20 \text{ M}\Omega$ in order to minimize its leakage.

For calculating R_6 we use the following equation:

$$R_6 = \left(\frac{V_{BG}}{V_{EOC}} \right) \cdot R_{OUT(TOT)} \quad (5.21)$$

where:

- R_6 → Lower resistor, connected to *EOC* and *GND*
- V_{BG} → Internal Bandgap voltage (1.23V, typical value)
- V_{EOC} → Maximum voltage in the battery before cutoff (4.2V in our case)
- $R_{OUT(TOT)}$ → Total output resistance, chosen previously.

By substituting our values in this equation, we obtain the following value:

$$R_6 = \left(\frac{1.23}{4.2} \right) \cdot 12.8 \cdot 10^6 = 3.749 \cdot 10^6 \Omega \equiv 3.75 M\Omega \quad (5.22)$$

The E24 normalized value will be $\mathbf{R_6 = 3.9 M\Omega}$.

Next, we calculate the value of R_5 by using the following equation:

$$R_5 = \left(\frac{V_{BG}}{V_{UVP}} \right) \cdot R_{OUT(TOT)} - R_6 \quad (5.23)$$

where:

- $\mathbf{R_5}$ → Middle resistor, connected to *EOC* and *UVP*
- $\mathbf{V_{BG}}$ → Internal Bandgap voltage (1.23V, typical value)
- $\mathbf{V_{UVP}}$ → Minimum voltage in the battery before cutoff (2.75V in our case)
- $\mathbf{R_{OUT(TOT)}}$ → Total output resistance, chosen previously
- $\mathbf{R_6}$ → R_6 value, calculated previously (3.9 M Ω)

By substituting our values in this equation, we obtain the following value:

$$R_5 = \left(\frac{1.23}{2.75} \right) \cdot 12.8 \cdot 10^6 - 3.9 \cdot 10^6 = 1.825 \cdot 10^6 \equiv 1.83 M\Omega \quad (5.24)$$

The E24 normalized value will be $\mathbf{R_5 = 1.8 M\Omega}$

Finally, we calculate R_4 by subtracting the R_5 and R_6 from the $R_{OUT(TOT)}$ value:

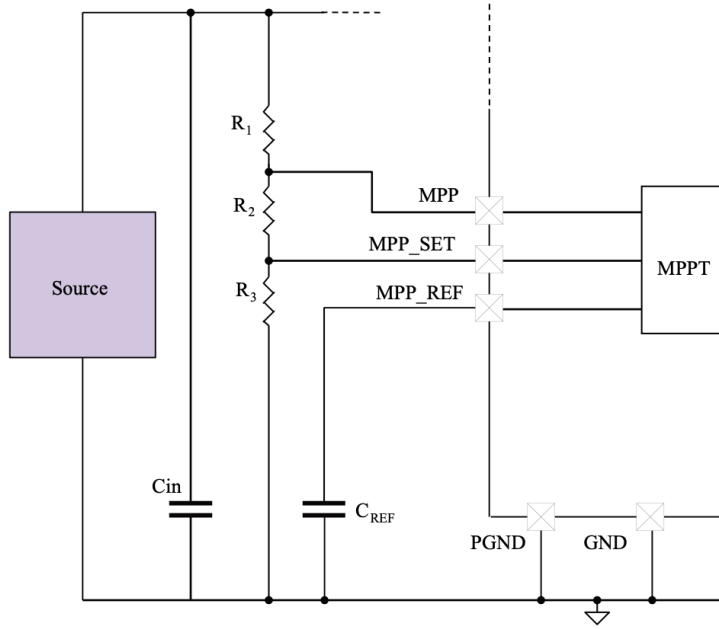
$$R_4 = R_{OUT(TOT)} - R_6 - R_5 = 7.1 \cdot 10^6 \equiv 7.1 M\Omega \quad (5.25)$$

We will take the E24 normalized value $\mathbf{R_4 = 6.8 M\Omega}$.

Finally, for the capacitor connected to the *STORE* output, we chose $\mathbf{C_{STORE} = 47\mu F}$, which is a typical application value according to the datasheet

MPPT Setting

Finally, we calculate the components connected to the part of the IC dedicated to manage the input from the PV panel and the MPPT algorithm. Just like the previous section, this part of the circuit consists of 3 resistors, but here we add 2 capacitors instead of one, as we can see on the following image (figure 33):



AM03400

Figure 33: Close-up view of the components in the MPPT setting section

Firstly, according to the datasheet, we need to select the values of the resistor following the next requirement

$$R_{IN(TOT)} = R_1 + R_2 + R_3 > \left(\frac{V_{OC(MAX)}}{I_{LEAKAGE}} \right) \cdot MPPT_{RATIO} \quad (5.26)$$

where:

- $R_{IN(TOT)}$ → Total input resistance
- R_1, R_2, R_3 → Resistors of the circuit
- V_{OC} → Maximum open circuit voltage of the PV panel (5.5V in our case)
- $I_{LEAKAGE}$ → Maximum acceptable leakage current, assumed 0.1 μ A as specified in the datasheet
- $MPPT_{RATIO}$ → MPPT ratio, calculated as V_{MP}/V_{OC} , where V_{MP} is the voltage at maximum power of the PV panel

For the next sections, we chose the value for $R_{in(out)}$ as follows:

$$R_{IN(TOT)MIN} = \frac{V_{OC(MAX)}}{I_{LEAKAGE}} \cdot MPPT_{RATIO} = \frac{5.5}{0.1 \cdot 10^{-6}} \cdot 0.691 = 38 \cdot 10^6 \equiv 38M\Omega \quad (5.27)$$

In order to calculate the values of all the resistors, we start by calculating R_1 :

$$R_1 = R_{IN(TOT)} \cdot \left[\left(\frac{V_{MPP(MAX)}}{V_{OC(MAX)}} \right) \right] \quad (5.28)$$

where:

- \mathbf{R}_1 → Upper resistor, connected between IN_HV and MPP
- $\mathbf{R}_{IN(TOT)}$ → Total input resistance, previously set to 38 M Ω
- $\mathbf{V}_{MPP(MAX)}$ → Voltage at maximum power of the PV panel (3.8V in our case)
- \mathbf{V}_{OC} → Maximum open circuit voltage of the PV panel (5.5V in our case)

By substituting our data, we obtain the following value:

$$R_1 = 38 \cdot 10^6 \cdot \left[\left(\frac{3.8}{5.5} \right) \right] = 24.87 \cdot 10^6 \equiv 24.87M\Omega \quad (5.29)$$

The closest E24 normalized resistor value is $\mathbf{R}_1 = \mathbf{24 M\Omega}$.

Next, for R_2 , we proceed as follows:

$$R_2 = R_{IN(TOT)} \cdot \left(\frac{V_{MPP(MAX)}}{V_{OC(MAX)}} \right) * (1 - MPPT_{RATIO}) \quad (5.30)$$

where:

- \mathbf{R}_2 → Middle resistor, connected between MPP and MPP_SET
- $\mathbf{R}_{IN(TOT)}$ → Total input resistance, previously set to 38 M Ω
- $\mathbf{V}_{MPP(MAX)}$ → Voltage at maximum power of the PV panel (3.8V in our case)
- \mathbf{V}_{OC} → Maximum open circuit voltage of the PV panel (5.5V in our case)
- $\mathbf{MPPT_{RATIO}}$ → MPPT ratio, calculated previously as V_{MP}/V_{OC}

Substituting our data, we obtain the following value:

$$R_2 = 38 \cdot 10^6 \cdot \left(\frac{3.8}{5.5} \right) \cdot (1 - 0.691) = 4.06 \cdot 10^6 \equiv 4.06 M\Omega \quad (5.31)$$

We selected a normalized E24 value $\mathbf{R_2 = 3.9 M\Omega}$.

Finally, we obtained the R_3 resistor as follows:

$$R_3 = R_{IN(TOT)} \cdot \left(\frac{V_{MPP(MAX)}}{V_{OC(MAX)}} \right) \cdot MPPT_{RATIO} \quad (5.32)$$

where:

- $\mathbf{R_3}$ → Lower resistor, connected between MPP_SET and GND
- $\mathbf{R_{IN(TOT)}}$ → Total input resistance, previously set to 38 M Ω
- $\mathbf{V_{MPP(MAX)}}$ → Voltage at maximum power of the PV panel (3.8V in our case)
- $\mathbf{V_{OC}}$ → Maximum open circuit voltage of the PV panel (5.5V in our case)
- $\mathbf{MPPT_{RATIO}}$ → MPPT ratio, calculated previously as V_{MP}/V_{OC}

This, applied to our data, results in the following value:

$$R_3 = 38 \cdot 10^6 \cdot \left(\frac{3.8}{5.5} \right) \cdot 0.691 = 9.07 \cdot 10^6 \equiv 9.07 M\Omega \quad (5.33)$$

The closest E24 normalized value for this resistor will be $\mathbf{R_3 = 10 M\Omega}$.

Now that we have the three values, we can check if they fulfill the first requirement, explained in equation (5.26):

$$R_{IN} = R_1 + R_2 + R_3 = 37.9 M\Omega \approx 38 M\Omega (R_{IN(MIN)}) \quad (5.34)$$

The resistor values follow the requirement.

Selection of the rest of components

For the capacitor C_{in} , we chose a $4.7\mu\text{F}$ value, as indicated in the datasheet:

Also, the MPPT accuracy can be strongly affected by an improper selection of the input capacitor. The input capacitance $C_{IN} = 4.7\mu\text{F}$ generally covers the most typical use cases.

(STMicroelectronics, SPV1050 Datasheet)

For the capacitor C_{REF} , we chose a 10nF value, also indicated by the datasheet:

When MPPT function is required, connect this pin to a 10nF capacitor: at every sampling period ($\hat{16}$ s) this capacitor stores the reference voltage (% of the open circuit voltage of the source) $VMPP_REF$.

(STMicroelectronics, SPV1050 Datasheet)

Finally, for the input inductor, the one connected between the positive terminal of the PV panel and the IN_LV pin, we chose a value of $22\mu\text{H}$, as indicated in the application diagram.

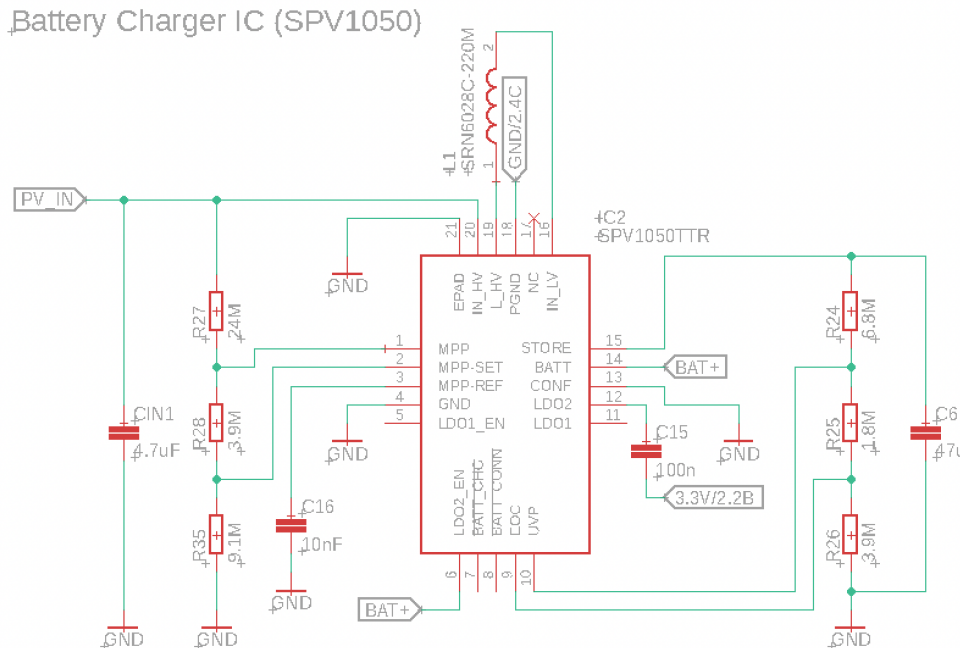


Figure 34: Schematic diagram of the SPV1050 assembly in *Eagle*

We can see the components placed in the PCB render below (figure 35):

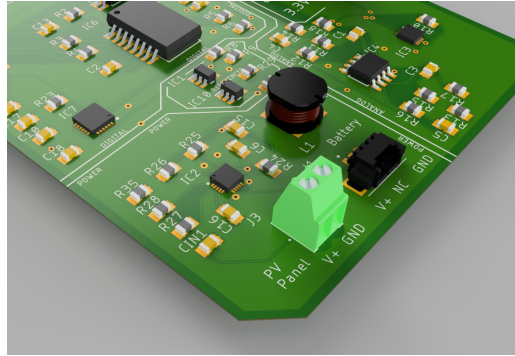
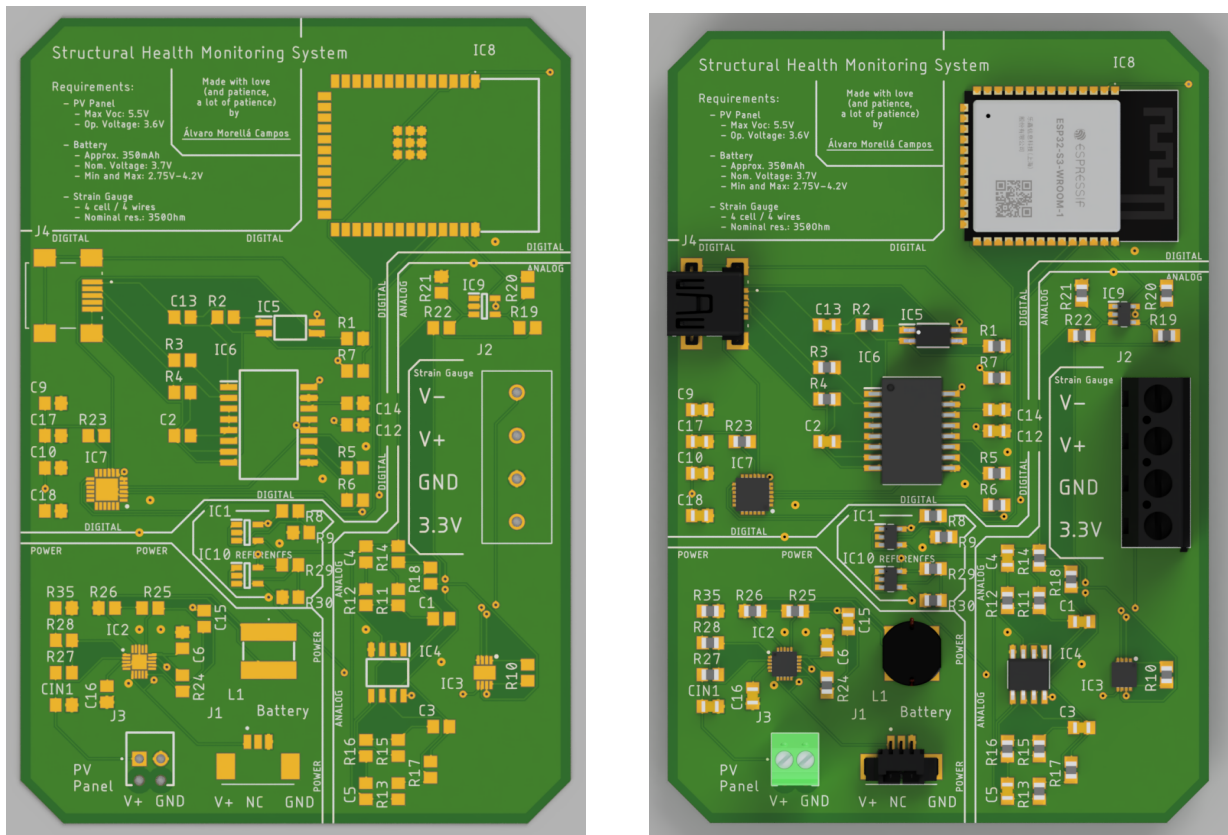


Figure 35: Render of the Power circuit in *Fusion360*

5.5 PCB

Once we placed all the components in the board in Eagle, we linked all the 3d models and these are the results of the renders:



(a) View of the PCB and soldering pads

(b) Components placed on the board

Figure 36: Fusion 360 Renders of the PCB

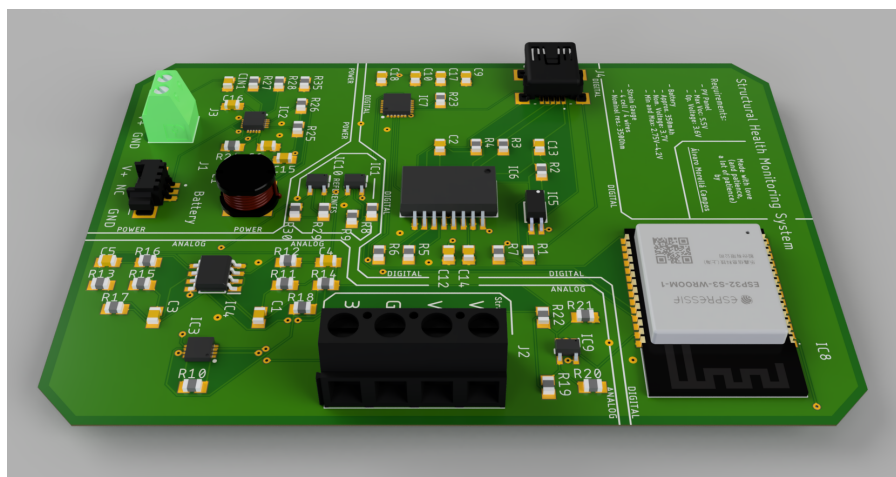


Figure 37: Side view render of the PCB in *Fusion360*

6 | Conclusions

6.1 Note from the author

The project here developed is a system envisioned for a real application in the bridge. However, the physical development of the project is to be realized.

We would also like to mention the different problems we encountered. For example, in the previous work of investigating the bridge construction, we found many articles about the general aspects of cable-stayed bridges. Moreover, we found a construction report from the subcontracted company that took care of the assembly of the bridge in which we found some information around the dimensions and construction. However, this was not enough for the initial data of our system, as we needed to know the exact value of the prestressing of the cables to set a "zero point" for the system. Some assumptions and approximations had to be carried out, which means that should it be constructed, further information around these values would be required.

On the other hand, for the design of the circuit, specially the power circuit, we encountered several problems in choosing the approach for design and assembly. A tailored DC-DC converter was intended as a first approach, but due to complications in the compatibility between the different parts of the system, an Integrated Circuit was finally chosen, which improved the reliability of the circuit while reducing its complexity.

Having stated that, we have to say that we are content with the final result of the system.

6.2 Future work

As previously stated, the design of this project has been carried out as a concept for future real implementation. However, for this to be feasible, some further work has to be done:

Regarding to the testing of the PCB, a prototype would be necessary to verify the correct operation of the circuit.

Finally, in terms of programming, we considered the software implementation of of the ESP32 μ Controller to be out of the scope of this project. However, it is an interesting part that will be carried out in the future. For real implementation, this part is necessary in order to ensure correct measurements and transmission of data.

6.3 Sustainable Development Goals

To conclude this report, we found interesting to mention the Sustainable Development Goals proportioned by the United Nations Organization that this project fulfills. These goals are the following:

- Goal 9 (Industry, innovation and infrastructure) as this project is intended to better the technology used in the industry and improve the design and construction of future infrastructures.
- Goal 11 (Sustainable cities and communities) as this project looks towards the safety of day-to-day used infrastructures while maintaining a sustainable energy use for this purpose

Bibliography

- [1] ABLIC, “Resistance to soldering heat condition for Package.” <https://www.ablic.com/en/semicon/support/package/solder-temp-profile/>, 2016.
- [2] C. R. Farrar and K. Worden, “An introduction to structural health monitoring an introduction to structural health monitoring,” *Philosophical Transactions of the Royal Society*, vol. 365, pp. 303–315, 2007.
- [3] J. Tondut, A. Gaymard, C. Zhou, and J. Chase, “Model creation using shm results for risk assessment in the subsequent earthquakes,” 04 2019.
- [4] G. Comanducci, F. Ubertini, and A. L. Materazzi, “Structural health monitoring of suspension bridges with features affected by changing wind speed,” *Journal of Wind Engineering and Industrial Aerodynamics*, vol. 141, pp. 12–26, 2015.
- [5] H. Li and J. Ou, “The state of the art in structural health monitoring of cable-stayed bridges,” *Journal of Civil Structural Health Monitoring*, vol. 6, 05 2015.
- [6] Vacker, “Structural Health Monitoring for Bridges, Buildings, Towers.” <https://www.vackergroup.ae/our-products/monitoring-systems/structural-health-monitoring/>, 2015.
- [7] N. A. J. Lieven, D. J. Ewins, C. R. Farrar, S. W. Doebling, and D. A. Nix, “Vibration-based structural damage identification,” *Philosophical Transactions of the Royal Society of London. Series A: Mathematical, Physical and Engineering Sciences*, vol. 359, no. 1778, pp. 131–149, 2001.
- [8] J. W. Matiko and S. P. Beely, *Applications of Energy Harvesting Technologies in Buildings*. Artech House, 2018.
- [9] A. Kingatua, “The How and Why of Energy Harvesting for Low-Power Applications.” <https://www.allaboutcircuits.com/technical-articles/how-why-of-energy-harvesting-for-low-power-applications/>, 2016.
- [10] A. Harb, “Energy harvesting: State-of-the-art,” *Renewable Energy*, vol. 36, no. 10, pp. 2641–2654, 2011.
- [11] T. Barcelo, “Energy Harvesting with Low Power Solar Panels.” <https://www.analog.com/en/technical-articles/energy-harvesting-with-low-power-solar-panels.html>, 2013.
- [12] National Instruments, “Maximum Power Point Trackers.” <https://web.archive.org/web/20110416062158/http://zone.ni.com/devzone/cda/tut/p/id/8106>, 2009.
- [13] Atonometrics, “What is a PV Module IV Curve?.” <https://www.atonometrics.com/applications/what-is-a-pv-module-iv-curve/>, 2023.

- [14] D. Beriber and A. Talha, “Mppt techniques for pv systems,” 05 2013.
- [15] Y. Jung, J. So, G. Yu, and J. Choi, “Improved perturbation and observation method (ip&o) of mppt control for photovoltaic power systems,” pp. 1788 – 1791, 02 2005.
- [16] V. Salas, E. Olías, A. Lazaro, and A. Barrado, “New algorithm using only one variable measurement applied to a maximum power point tracker,” *Solar Energy Materials and Solar Cells*, vol. 87, pp. 675–684, 05 2005.
- [17] R. Hilloowala and A. Sharaf, “A rule-based fuzzy logic controller for a pwm inverter in photo-voltaic energy conversion scheme,” pp. 762 – 769 vol.1, 11 1992.
- [18] D. Delso, “Azud del Oro bridge and The Agora, City of Arts and Sciences, Valencia, Spain..” https://commons.wikimedia.org/wiki/File:%C3%81gora,_Ciudad_de_las_Artes_y_las_Ciencias,_Valencia,_Espa%C3%B1a,_2014-06-29,_DD_58_alt.jpg, 2014.
- [19] L. Viñuela and J. Martínez, “L’Assut de l’Or Bridge (Serrería bridge), Valencia, Spain,” *Revista trimestral de la Asociación Científico-Técnica del Hormigón Estructural (ACHE)*, vol. 60 - n^o254, pp. 7–28, 2009.
- [20] P. Cawley and R. D. Adams, “The location of defects in structures from measurements of natural frequencies,” *The Journal of Strain Analysis for Engineering Design*, vol. 14, no. 2, pp. 49–57, 1979.
- [21] S. Kangas, A. Helmicki, V. Hunt, R. Sexton, and J. Swanson, “Cable-stayed bridges: Case study for ambient vibration-based cable tension estimation,” *Journal of Bridge Engineering*, vol. 17, no. 6, pp. 839–846, 2012.
- [22] R. Tinder, *Relativistic Flight Mechanics and Space Travel: A Primer for Students, Engineers and Scientists*. Synthesis lectures on engineering, Morgan & Claypool Publishers, 2007.
- [23] S. Keil, *Fundamentals of strain gage technology*, ch. 2, pp. 17–108. John Wiley & Sons, Ltd, 2017.
- [24] T. Nachazel, “¿Qué es una galga extensométrica y cómo funciona?.” <https://es.michsci.com/what-is-a-strain-gauge/?cn-reloaded=1>, 2020.
- [25] D. M. Ștefănescu, *Wheatstone Bridge - The Basic Circuit for Strain Gauge Force Transducers*, pp. 347–360. Berlin, Heidelberg: Springer Berlin Heidelberg, 2011.
- [26] National Instruments, “Application note 078.” <http://www.ing.unp.edu.ar/electronica/assignaturas/ee016/anexo/r-an078.pdf>, 2023.
- [27] Pfeifer, “Wire Ropes - Technical Information.” https://www.pfeifer.info/out/assets/PFEIFER_WIRE-ROPES-TECHNICAL-INFO_PPEN.PDF, 2020.
- [28] IPC, “Qualification and Performance Specification for Rigid Printed Boards,” standard, IPC, Illinois, USA, Mar. 2020.
- [29] IPC, “Standard for Determining Current-Carrying Capacity In Printed Board Design,” standard, IPC, Illinois, USA, Mar. 2020.
- [30] IPC, “Generic Standard on Printed Board Design,” standard, IPC, Illinois, USA, Mar. 2020.

- [31] E. Parliament, “Directive 2011/65/EU of the European Parliament and of the Council of 8 June 2011 on the restriction of the use of certain hazardous substances in electrical and electronic equipment,” standard, European Parliament and Council, Brussels, BE, 2011.
- [32] talent.com, “Salario medio para Ingeniero Electronico en España, 2023.” [https://es.talent.com/salary?job=ingeniero+electronico#:~:text=El%20salario%20ingeniero%20electronico%20promedio,hasta%20%E2%82%AC%2037.800%20al%20a%C3%B1o.](https://es.talent.com/salary?job=ingeniero+electronico#:~:text=El%20salario%20ingeniero%20electronico%20promedio,hasta%20%E2%82%AC%2037.800%20al%20a%C3%B1o.,), 2023.

Part II

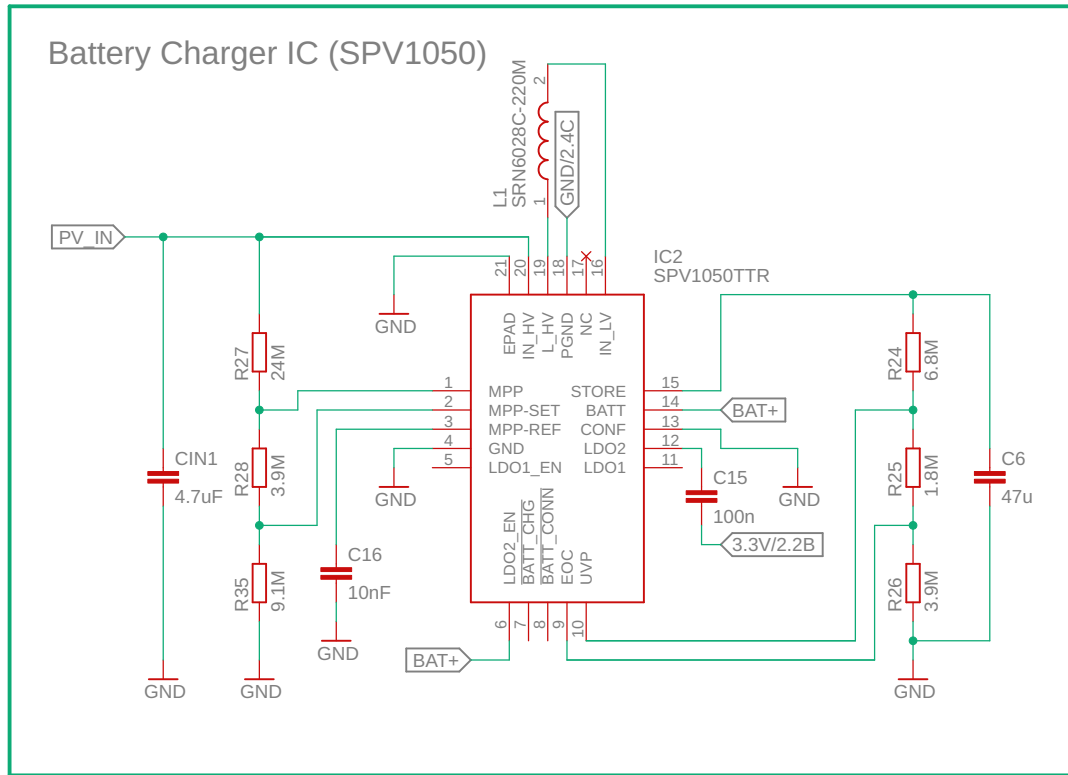
Plans

Index of the Plans

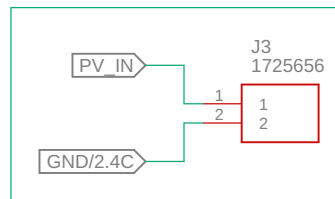
1	Diagrams of the electronics system	70
1.1	Schematics of the power circuit	70
1.2	Schematics of the conditioning circuit	72
1.3	Schematics of the processing circuit (ESP32)	74
2	PCB layout diagrams	76
2.1	Front Silkscreen	76
2.2	Front Layer	78
2.3	Back Layer	80

1 | Diagrams of the electronics system

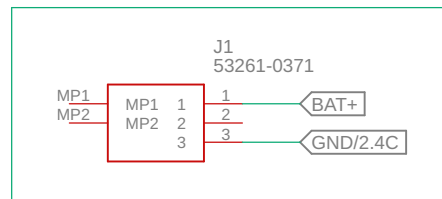
1.1 Schematics of the power circuit



PV Panel connector



Battery connector



SHM signal processing system

Power circuit:
Implementation of
the SPV1050 IC
and connectors

ÁLVARO MORELLÁ CAMPOS

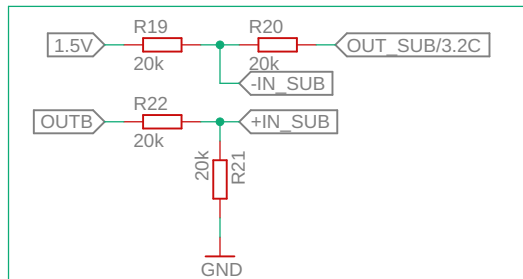
TFG_Schematic

25/07/2023 10:20

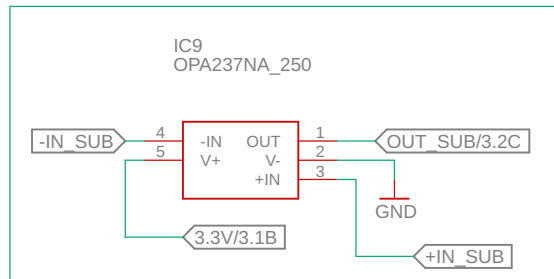
Sheet: 1/3

1.2 Schematics of the conditioning circuit

Offset subtractor

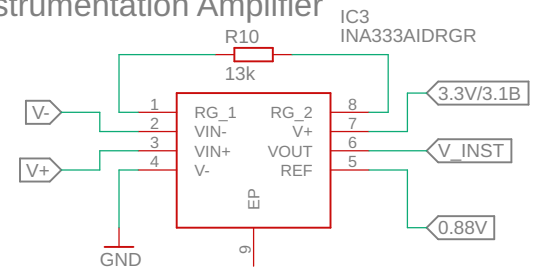


Subtractor resistors

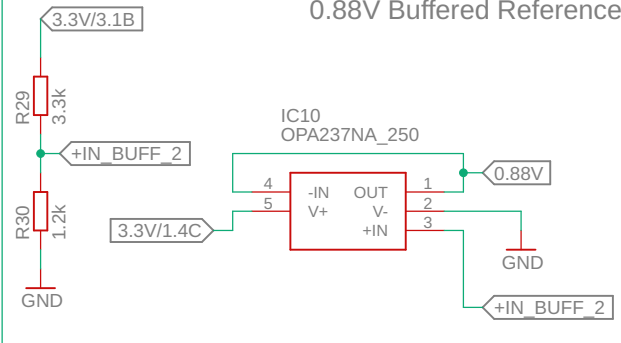


Operational Amplifier (OPA237, Texas Inst.)

Instrumentation Amplifier

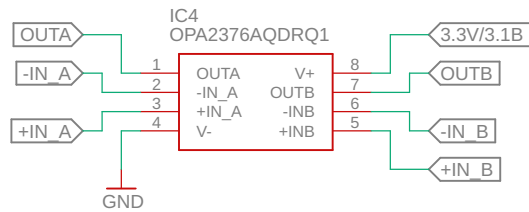


0.88V Buffered Reference

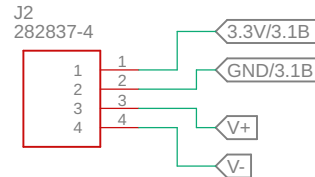


Low Pass Filter (30Hz)

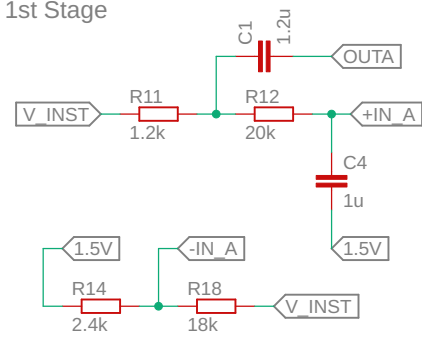
Double Op Amp (OPA2376, Texas Inst.)



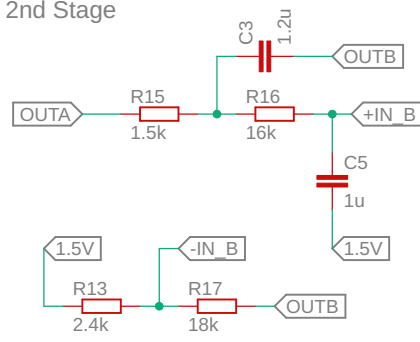
Gauge connection



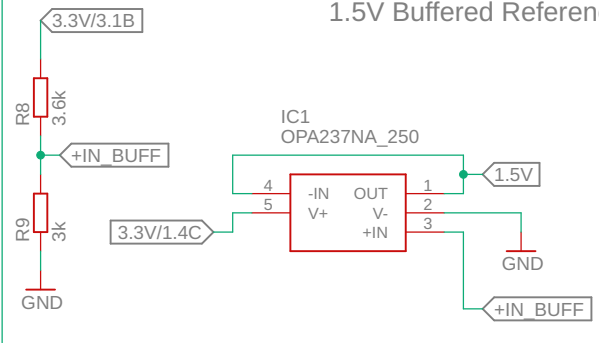
1st Stage



2nd Stage



1.5V Buffered Reference



SHM signal processing system

Analog circuit:
Implementation of
the conditioning
stages of the system

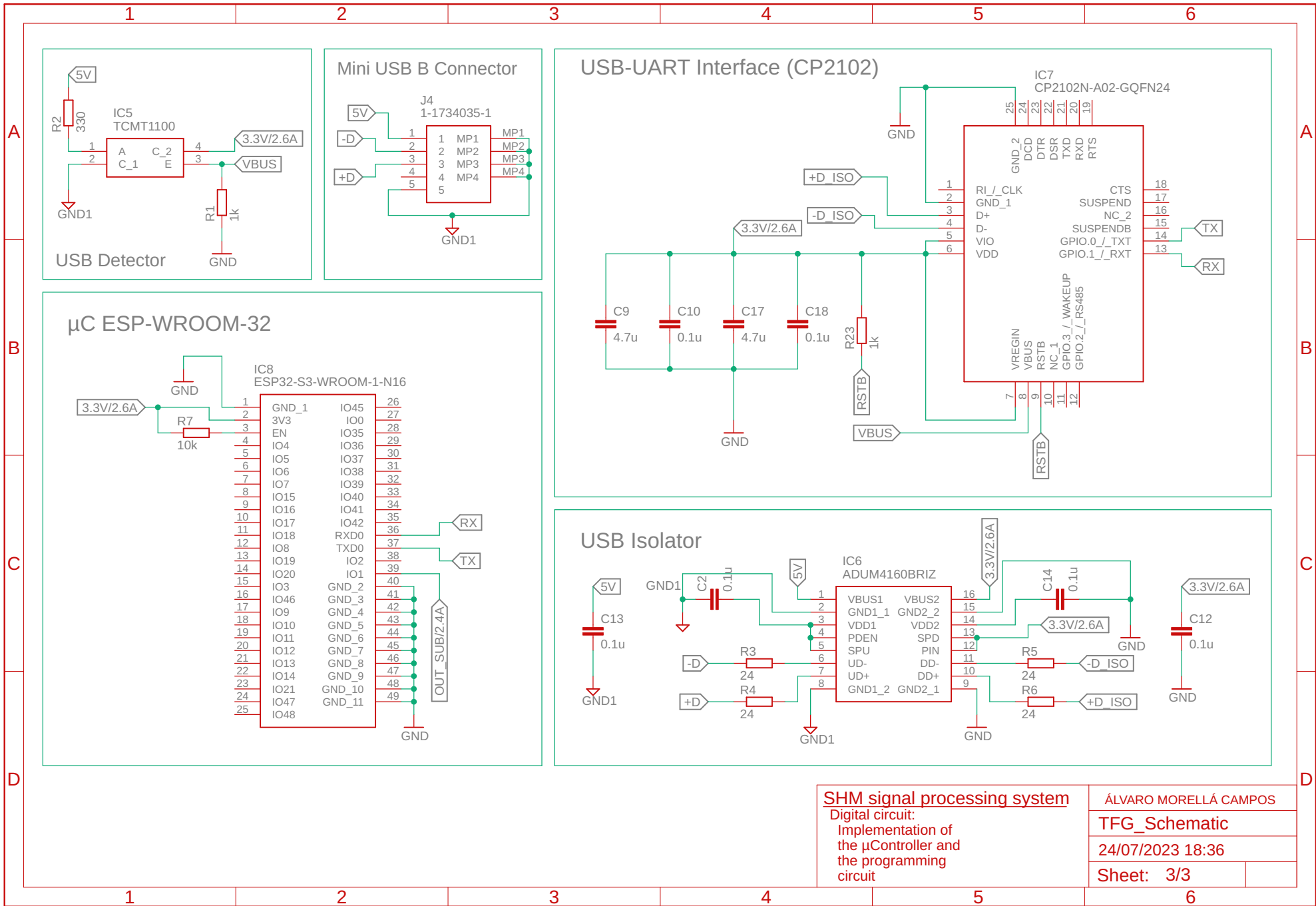
ÁLVARO MORELLÁ CAMPOS

TFG_Schematic

24/07/2023 18:36

Sheet: 2/3

1.3 Schematics of the processing circuit (ESP32)



SHM signal processing system

Digital circuit:
 Implementation of
 the µController and
 the programming
 circuit

ÁLVARO MORELLÁ CAMPOS

TFG_Schematic

24/07/2023 18:36

Sheet: 3/3

2 | PCB layout diagrams

2.1 Front Silkscreen

1

2

3

4

A

A

B

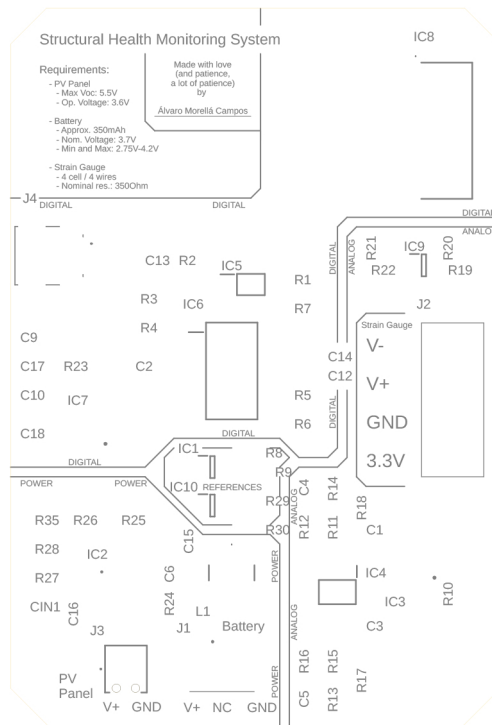
B

C

C

D

D



SHM signal processing system

ÁLVARO MORELLÁ CAMPOS

TFG_Board

Front Silkscreen

24/07/2023 19:55

Sheet: 1/3

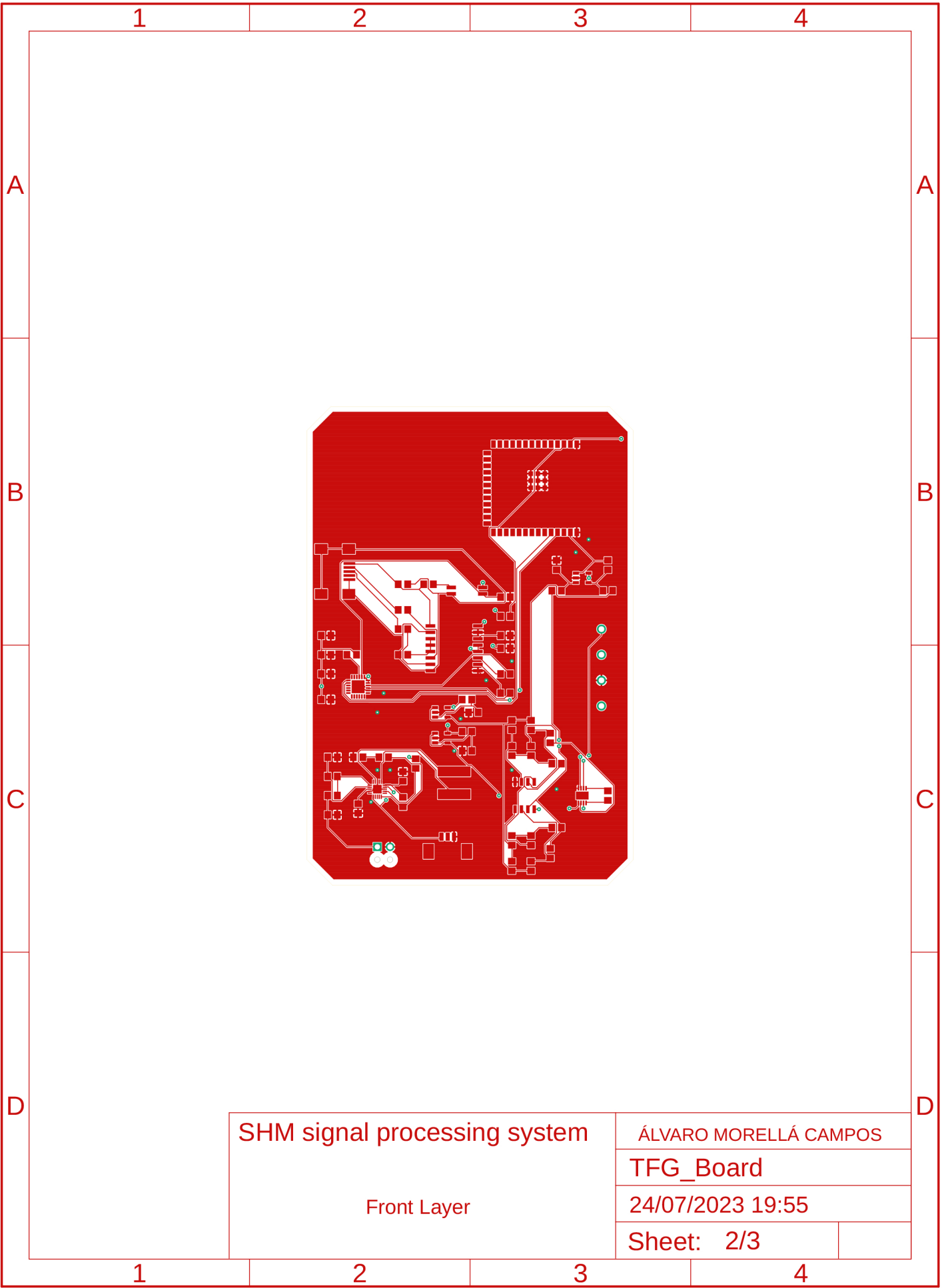
1

2

3

4

2.2 Front Layer

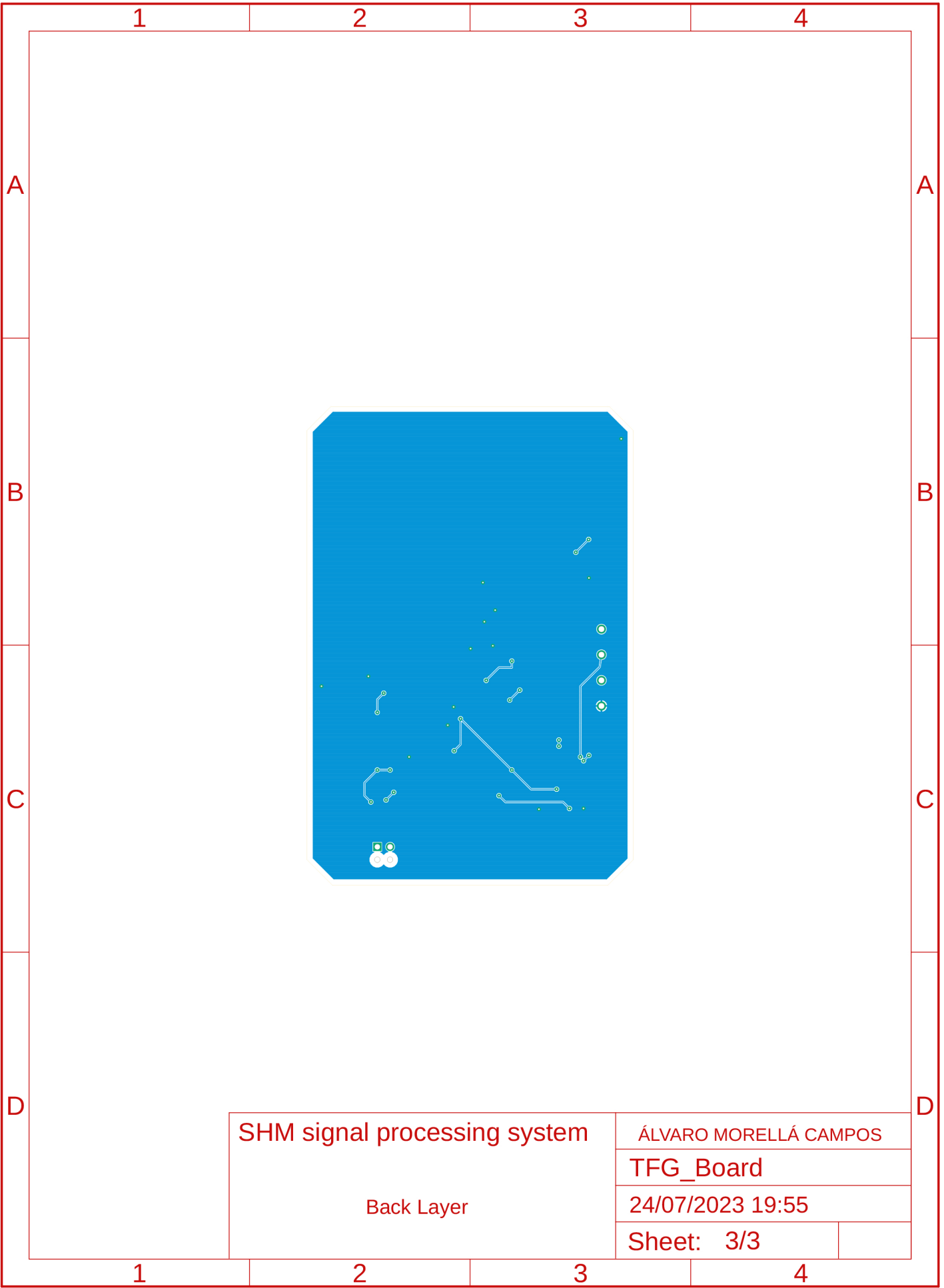


SHM signal processing system

Front Layer

ÁLVARO MORELLÁ CAMPOS	
TFG_Board	
24/07/2023 19:55	
Sheet: 2/3	

2.3 Back Layer



SHM signal processing system

Back Layer

ÁLVARO MORELLÁ CAMPOS	
TFG_Board	
24/07/2023 19:55	
Sheet: 3/3	

Part III

Written specifications

Index of the Written Specifications

1	Introduction	85
1.1	Scope of the document	85
1.2	Intended audience	85
2	General requirements and considerations	87
2.1	Materials	87
2.1.1	Strain Gauge	87
2.1.2	PCB	88
2.1.3	Electronic components	88
3	Fabrication	89
3.1	PCB Assembly	89
4	Testing	91
4.1	Necessary equipment	91
4.2	Electrical components	91
4.2.1	Battery	91
4.2.2	PV Panel	91
4.3	Strain Gauge	92
4.4	PCB	92

1 | Introduction

This document is part of the design of a Structural Monitoring System based on the concept of Energy Harvesting. It is intended to be installed in the stay-cables of the *Assut de l'Or* bridge in Valencia, Spain. The device is intended for safety measures as well as for the implementation of a mathematical model of the bridge for future study.

1.1 Scope of the document

The aim of this document is to establish the technical standards this project needs to fulfill so as to be correctly replicated and implemented. It consists on the minimum requirements to be followed in order to correctly develop the system described in the Technical Report and the Plans.

1.2 Intended audience

This document is intended to be read by the engineers or technicians responsible for manufacturing and implementing the device should it be physically developed. This document should be taken into account together with the rest of sections of the thesis (Technical Report, Plans and Budget).

2 | General requirements and considerations

In this chapter, the general requirements will be assessed so as to inform of the specifications and techniques that should be followed in the implementation of this system.

2.1 Materials

In this section, the specifications and regulations that the materials used have to follow will be presented.

2.1.1 Strain Gauge

In this project, an *OMEGA SGT-3G/350-FB41* strain gauge has been used. However, due to the standardization of this kind of components, other gauges can be implemented.

For a whole compatibility with the system, the strain gauge used needs to follow the following requirements:

- Nominal resistance of 350Ω
- Four measuring grids (2 at 90° respect to the other two)
- Epoxy installation or spot weldable
- Temperature compensation for steel

Following these specifications, there should be no problem with the usage of other gauges.

2.1.2 PCB

- The PCB designed in this project is formed by two copper layers of 35 μm and a core layer of 150 μm .
- The silkscreen must be painted in a high contrast color depending on the color of the PCB. In this case, white is the most appropriate color.
- The design and manufacturing of the PCBs has to follow norm IPC 6012E, which specifies the quality and performance specifications of rigid printed boards [28].
- The design and manufacturing of the PCBs has to follow norm IPC 2152, which defines the standards for current carrying capacity of printed circuit boards [29].
- The design and manufacturing of the PCBs has to follow norm IPC 2220, which sets the standards for general PCB design [30].

2.1.3 Electronic components

All the components used in the assembly of this project have been thoroughly calculated and their values should not be modified unless specified by the engineer in charge of the design.

All electronic components have to be provided with a RoHS [31] certificate of compliance.

3 | Fabrication

In this section, we will specify the minimum requirements for the fabrication and assembly of the system

3.1 PCB Assembly

For the assembly of the PCB, a certified technician or assembling company will be needed. The former should provide an IPC-A-610E compliance document.

A lead-free solder paste must be used for the assembly of the Surface Mount Device (SMD) components so as to comply with the RoHS[31] directive.

For the through-hole components, a lead-free wire should be used so as to comply with the previously mentioned normative.

Finally, for the soldering of the components, an acceptable temperature profile should be used. It should look as the following one in figure 38:

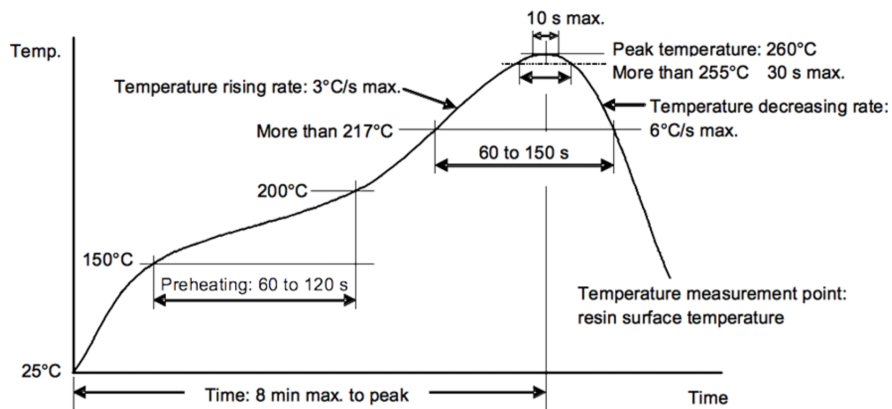


Figure 38: Temperature profile for reflux soldering of PCBs [1]

4 | Testing

In this chapter of the document, we will explain general recommendations for the testing of the different components of the system. For a correct implementation, refer to this section before assembling all the parts and check their operation.

4.1 Necessary equipment

For the testing of the equipment, a computer will be needed so as to implement the code in the μ Controller and to check the data sent by the ESP32 Wi-Fi functionality.

Also a multimeter will be needed so as to measure the different electric values of the components that will be installed.

4.2 Electrical components

In this section, we will indicate the procedure for testing the components of the system.

4.2.1 Battery

The testing of the battery should be done according to the datasheet provided. The battery voltage should be tested with a multimeter so as to check that the minimum value is reached. On the contrary, there could be a failure on the battery.

A charge test should also be performed, so as to check if the battery can remain charged for the specified time and if it can hold as much energy as indicated in the specifications.

4.2.2 PV Panel

For testing the PV panel, the open circuit voltage should be measured with a multimeter. The value specified in the datasheet should appear in the multimeter display.

Check the connections between the terminals of the panel in case there is not a normal reading of the voltage.

4.3 Strain Gauge

Check that the nominal resistance is approximately $350\ \Omega$ in all grids. The response to a force will be difficult to measure, as these strain gauges are prepared to support extremely high strains.

4.4 PCB

A visual inspection of the PCB can be performed. Once the components of the board are installed, a test of the functions can be performed so as to check the correct operation of the system. Specially the response from the Power IC, the SVP1050, and its response to the first connection to the PV panel and battery (check that it charges the battery correctly).

Part IV

Budget

Index of the Budget

1	Price of the project development	95
1.1	Designer's fees	95
1.1.1	Hour breakdown	95
1.2	Budget of materials	96
1.2.1	Electronics components	96
1.2.2	PCB Manufacturing	98
1.3	Amortization of tools and programs	98
2	Conclusion (Total Price)	101
3	Price per unit of production	103
3.1	Budget of materials	103
3.2	Price per unit	103

1 | Price of the project development

In this section, we will calculate the prices of the labor, the materials and the equipment utilized in this project.

For the first part, we calculated an approximation of the hours spent in the design of this project, while for the second part, we used the prices specified in each provider's website, all of them without Value Added Tax (VAT, or IVA in Spain).

1.1 Designer's fees

According to what has been investigated through different web pages in the Internet, the average salary of an engineer in Spain in 2023 is approximately 15.38 [32].

With this value in mind, we can now calculate the hours spent in this project and how this reflects on the economical cost of the project.

1.1.1 Hour breakdown

In the following table (table 1.1), we can see an approximation of how the hours have been divided:

Hours of work (breakdown)			
Item	Hours	Total in h	Total in €
Electronics design		190	2922.2
Calculations	80		
Eagle Schematics	50		
PCB Layout	60		
Mechanical design		20	307.6
3D Design (PCB)	20		
Documentation		150	2307
Thesis	120		
Plans	20		
Budget	10		
	TOTAL	360	5536.8€

Table 1.1: Breakdown of the hours spent in this project and its economical correspondence

We can see that the total labor cost of the project for approximately 360h is **5536.8€**

1.2 Budget of materials

In this section, we will include a breakdown of all the prices of the components used in this project according to the provider's web page. We will also include the price of manufacture of a PCB.

1.2.1 Electronics components

In this section, the price of each component is specified and calculated for the total units needed for the project. It is important to have in mind that these prices are for the units specified, meaning that the provider might apply a discount for bigger units.

We will see this in the final section of this document, where we will calculate the price for the total number of devices manufactured (30).

Electronic components						
#	Type	Reference	Qty.	Provider	Unit Price (no VAT)	Subtotal (no VAT)
1	Capacitor	C0805C104K5RAC7411	7	MOUSER	0.09 €	0.63 €
2	Capacitor	C0805C125K9RACTU	2	MOUSER	0.52 €	1.04 €
3	Capacitor	C0805C476M9PACTU	1	MOUSER	0.68 €	0.68 €
4	Capacitor	C0805C824K4RACAUTO	1	MOUSER	0.27 €	0.27 €
5	Capacitor	C0805X105K8RACAUTO	1	MOUSER	0.57 €	0.57 €
6	Capacitor	C0805X475J4RACAUTO	3	MOUSER	0.58 €	1.74 €
7	Resistor	CR0805-JW-102ELF	1	MOUSER	0.07 €	0.07 €
8	Resistor	CR0805-JW-103ELF	1	MOUSER	0.07 €	0.07 €
9	Resistor	CR0805-JW-122ELF	4	MOUSER	0.07 €	0.28 €
10	Resistor	CR0805-JW-133ELF	1	MOUSER	0.07 €	0.07 €
11	Resistor	CR0805-JW-152ELF	1	MOUSER	0.07 €	0.07 €
12	Resistor	CR0805-JW-163ELF	1	MOUSER	0.07 €	0.07 €
13	Resistor	CR0805-JW-183ELF	1	MOUSER	0.08 €	0.08 €
14	Resistor	CR0805-JW-185ELF	1	MOUSER	0.07 €	0.07 €
15	Resistor	CR0805-JW-203ELF	5	MOUSER	0.07 €	0.35 €

1.2. BUDGET OF MATERIALS

16	Resistor	CR0805-JW-240ELF	4	MOUSER	0.07 €	0.28 €
17	Resistor	CR0805-JW-242ELF	2	MOUSER	0.07 €	0.14 €
18	Resistor	CR0805-JW-302ELF	1	MOUSER	0.07 €	0.07 €
19	Resistor	CR0805-JW-331ELF	1	MOUSER	0.07 €	0.07 €
20	Resistor	CR0805-JW-332ELF	1	MOUSER	0.07 €	0.07 €
21	Resistor	CR0805-JW-362ELF	1	MOUSER	0.07 €	0.07 €
22	Resistor	CR0805-JW-395ELF	2	MOUSER	0.07 €	0.14 €
23	Resistor	CR0805-JW-685ELF	1	MOUSER	0.07 €	0.07 €
24	Resistor	CR0805-JW-915ELF	1	MOUSER	0.07 €	0.07 €
25	Resistor	MCHVR05JTHW2405	1	FARNELL	0.16 €	0.16 €
26	Inductor	SRN6028C-220M	1	MOUSER	0.38 €	0.38 €
27	Op Amp	OPA2376AQDRQ1	1	MOUSER	2.25 €	2.25 €
28	Op Amp	OPA237NA/250	1	MOUSER	1.60 €	1.60 €
29	Inst Amp	INA333AIDRGT	1	MOUSER	4.92 €	4.92 €
30	Power IC	SPV1050TTR	1	MOUSER	3.20 €	3.20 €
31	USB Isolator	ADUM4160BRIZ	1	MOUSER	10.38 €	10.38 €
32	USB to UART	CP2102N-A02-GQFN24	1	MOUSER	3.28 €	3.28 €
33	Optocoupler	TCMT1100	1	MOUSER	0.45 €	0.45 €
34	2 Pin Terminal	1725656	1	MOUSER	1.45 €	1.45 €
35	4 Pin Terminal	282837-4	1	MOUSER	0.85 €	0.85 €
36	Battery Connector	53261-0371	1	MOUSER	0.51 €	0.51 €
37	ESP32 µController	ESP32-S3- WROOM-1-N16R8	1	MOUSER	3.21 €	3.21 €
38	USB Conector	1-1734035-1	1	MOUSER	1.21 €	1.21 €
39	PV Panel	MPT3.6-75	1	MOUSER	5.50 €	5.50 €
40	Battery	YOBLP422339PACK	1	FARNELL	19.53 €	19.53 €
50	Strain Gauge	SGT-3G/350-FB41	1	OMEGA	30.91€	30.91€
					TOTAL (no VAT)	96.83 €

1.2.2 PCB Manufacturing

A professional PCB manufacturer was chosen. In this case, it will be *Aisler*.

The price for a board can be calculated as follows:

$$Price = 12 + 0.042 \cdot Area(cm^2) \quad (1.1)$$

In our case, the price for each PCB is **18.72€** (15.47€without VAT)

As an addition to the board, we can order a stencil for better distribution of the soldering paste, the price of which can be calculated as follows:

$$Price = 5 + 0.095 \cdot Area(cm^2) \quad (1.2)$$

In our case, the price for the stencil is **20.2€** (16.69€without VAT). This product, however, can be used almost indefinitely, as it's only used for application of the soldering paste.

For the assembly of the PCBs, we have counted on a work of 1.5h, which results in a total of **23.07€**. Added to the rest of the costs of fabrication, we obtain the total shown in the following table:

PCB Costs	
Item	Cost
PCB Board	18.72 €
Stencil	20.20 €
Assembly	23.07 €
TOTAL	61.99 €

Table 1.3: Total cost of the fabrication and assembly of the PCB

We obtain a final value for a PCB of **52.23€** without VAT.

1.3 Amortization of tools and programs

In this section, we calculated the amortization of the equipment and software used in this project.

The amortization ratio is calculated as follows:

$$Amortization_{ratio} = \frac{Price}{Service\ life} \quad (1.3)$$

1.3. AMORTIZATION OF TOOLS AND PROGRAMS

We can use this ratio to calculate the amortization of each of the elements used for the realization of the project, as we can see in the following table:

Amortization of equipment					
Item	Price	Service life	Amortization Ratio (€/h)	Hours	Total
MacBook Pro	2,500.00 €	60000	0.042	360	15.00 €
iPad 2018	400.00 €	44000	0.009	300	2.73 €
Fusion360/Eagle	382.00 €	8760	0.044	110	4.80 €
Mathcad	665.80 €	8760	0.076	60	4.56 €
Photoshop	600.00 €	8760	0.068	5	0.34 €
TOTAL					27.43€

Table 1.4: Amortization of the equipment and software

We can see that the total amortization of the equipment and software used comes to about 27.43€.

2 | Conclusion (Total Price)

The total gross cost of the project (including the labor, the material cost and the amortization) has been calculated in the following table:

Total cost of the project	
Item	Cost
PCB Components	96.83 €
PCB Manufacturing	55.23 €
Labor	5,536.80 €
Amortizations	27.43 €
GROSS TOTAL	5,716.29 €

Table 2.1: Total gross cost of the project

In order to calculate the net cost of the project, we added the 21% of VAT stipulated for Spain and an gain percentage of 8%, which is a good gain value. We can see this in the following table:

Net cost	
Parts	Cost
Gross total	5,716.29 €
VAT (21%)	1,200.42 €
Gains (8%)	457.30 €
TOTAL	7,374.01 €

Table 2.2: Net total cost of the project

The cost of the project comes to a net total of **7,374.01 €**.

3 | Price per unit of production

In this section of the budget we will calculate the price per unit of production. It is estimated to manufacture a total of 30 units of this product, one per cable of the bridge with one to spare in case there is a failure.

3.1 Budget of materials

As we previously stated in this document, the price for a bulk order makes the unit price considerably lower. In our case, with a bill of materials 30 times the initial calculations, we obtain a total of **2551.16 €** without VAT, which results in 85.04€/u.

In addition, as we explained for the manufacturing of the PCBs, the stencil will only be charged once, as it can be reused indefinitely. The total cost for the material part has been explained in the following table:

Material costs for 30 units			
Materials	Unit price	Quantity	Subtotal
Components	85.04 €	30	2551.2 €
PCB Fabrication	15.47 €	30	464.10 €
PCB Assembly	23.07 €	30	692.10 €
Stencil	16.69 €	1	16.69 €
TOTAL			3724.09 €
UNIT			124.14€/u.

The total for the 30 units production is **3724.09€**.

3.2 Price per unit

Accounting for a 30 unit production (one for each cable of the bridge plus one to spare), we calculated the gross total as follows:

Gross cost per unit	
Item	Cost per unit
Assembly	124.14 €
Labor	185.56 €
Amortization	0.91 €
GROSS TOTAL	310.61 €/u.

Table 3.2: Gross total per unit of a 30 unit production

Finally, we added a 21% of VAT and 8% of industrial gain. We also accounted for 8% more for fabrication installations costs (electricity and others):

Net cost per unit	
Part	Cost
Gross total	310.61 €
VAT	65.23 €
Gain	24.85 €
Installations	24.85 €
TOTAL	425.54 €

Table 3.3: Total cost per unit of a 30 unit production

The final Retail Price is **425.54€**.

